



Review

PEMFC Gas-Feeding Control: Critical Insights and Review

Shiyi Fang ¹, Jianan Feng ¹, Xinyu Fan ^{1,*}, Daifen Chen ¹  and Cao Tan ² 

¹ School of Energy and Power, Jiangsu University of Science and Technology, Zhenjiang 212100, China; shiyifang@stu.just.edu.cn (S.F.); jnfeng@stu.just.edu.cn (J.F.); dfchen@just.edu.cn (D.C.)

² School of Transport and Vehicle Engineering, Shandong University of Technology, Zibo 255100, China; njusttancao@yeah.net

* Correspondence: fanxy@just.edu.cn

Abstract: Proton exchange membrane fuel cells (PEMFCs) are currently a relatively mature type of hydrogen energy device due to their high efficiency and low noise compared to traditional power devices. However, there are still challenges that hinder the large-scale application of PEMFCs. One key challenge lies in the gas supply system, which is a complex, coupled nonlinear system. Therefore, an effective control strategy is essential for the efficient and stable operation of the gas control system. This paper aims to provide a comprehensive and systematic overview of the control strategies for PEMFC anode and cathode supply systems based on an analysis of 182 papers. The review covers modern control theories and optimization algorithms, including their design, objectives, performance, applications, and so on. Additionally, the advantages and disadvantages of these control methods are thoroughly evaluated and summarized.

Keywords: PEMFC; modeling and control strategies; decarbonized power system; hydrogen energy

1. Introduction

The development of green energy is accelerating globally, driven by government policies [1–4] that support the research, development, and application of green energy technologies [5–7]. These policies also encourage enterprises and individuals to adopt clean energy [8–11]. Despite the technical, economic, and policy challenges that green energy faces [12–15], it holds significant potential and represents a crucial direction for future energy development [16–19].

Hydrogen is considered a green energy source and a crucial component of the future energy transition, particularly in heavy industry and transportation [20–22]. It is a clean form of energy with high mass energy density. Meanwhile, hydrogen can be utilized either through combustion or by converting it into electricity using fuel cells [23,24]. Fuel cells outperform direct hydrogen combustion in several aspects, including efficiency, emissions, noise, flexibility, start-up speed, and maintenance [25,26]. Consequently, they are considered the superior choice for many applications [27–30]. Proton exchange membrane fuel cells (PEMFCs) are currently a relatively mature type of hydrogen energy device [31,32]. Despite their remarkable potential, PEMFCs face several limitations [33,34]. High cost, technical challenges related to hydrogen storage and transportation, and the complexity of systems needed to maintain suitable operating conditions are major obstacles. Among these limitations, the supply system is a complex and critical subsystem in the PEMFC system [35]. The gas content in the stack significantly affects the working efficiency of the PEMFC stack and can even cause irreversible damage. The regulation of air and fuel gas supply exerts a direct influence on the efficiency of the electrochemical reactions within the PEMFC stack. Meanwhile, during abrupt shifts of current, a failure of the supply system to respond promptly induces sudden pressure fluctuations within the stack. This can lead to an imbalance of pressure across the proton exchange membrane (PEM) in turn, potentially causing irreversible damage to the PEMFC. Thus, advanced control algorithms



Citation: Fang, S.; Feng, J.; Fan, X.; Chen, D.; Tan, C. PEMFC Gas-Feeding Control: Critical Insights and Review. *Actuators* **2024**, *13*, 455. <https://doi.org/10.3390/act13110455>

Academic Editor: Ioan Ursu

Received: 12 October 2024

Revised: 8 November 2024

Accepted: 12 November 2024

Published: 13 November 2024



Copyright: © 2024 by the authors. Licensee MDPI, Basel, Switzerland. This article is an open access article distributed under the terms and conditions of the Creative Commons Attribution (CC BY) license (<https://creativecommons.org/licenses/by/4.0/>).

are employed to promptly adjust the actuators within the supply system in response to disturbances, thereby enhancing system efficiency, stability, and service life, and ultimately decreasing operational costs. The exploration of control algorithms tailored for the supply system remains an active area of research.

In a prior review, P. Yang classified the control methodologies based on a comprehensive evaluation and summation of control strategies implemented in PEMFCs [36]. Nonetheless, it is noteworthy that within a given control category, there may exist diverse application subsystems in this review. D. Wu presents a thorough summary of extant research, encompassing modeling of fuel cell stacks, subsystem modeling, and their applications [37]. The multiphysics field modeling and engineering design of PEMFCs offer readers an insightful comprehension of the internal operational mechanisms of the PEMFC stack. Additionally, a concise description of the structure and control of individual subsystems is provided. Daud offered an in-depth discussion of the control subsystems of PEMFC, specifically focusing on reaction management, heat management, water management, and power electronics subsystems. Special attention is given to control strategies designed to prevent fuel overload [38]. X. Lu summarized recent comprehensive research on energy management strategies (EMS) for Proton Exchange Membrane Fuel Cell-Hybrid Electric Vehicle (PEMFC-HEV) hybrid power systems (HPS) [39]. The study centers on the EMS of PEMFCs serving as the primary power source for HEVs, with batteries and supercapacitors acting as auxiliary energy sources. It encompasses their classifications, respective advantages and disadvantages, along with the existing challenges and the control strategies implemented to address these issues. S. George presented several issues identified in recent reports on PEMFC modeling efforts and a correct model of the PEMFC with a detailed theoretical basis is given [40]. This study also reviews various applicable Maximum Power Point Tracking (MPPT) techniques and derives valuable results based on key parameters used to assess the performance of these methods. These review articles on PEMFC modeling, application, and control are inspiring for subsequent research. However, since PEMFCs are complex systems composed of several subsystems, these reviews tend to analyze them from a global perspective without delving deeply into the subsystems. Building on these insights, this paper offers a more in-depth and comprehensive review of various control strategies for PEMFC supply systems. Specifically, the performance and application conditions of different control methods will be comprehensively compared and evaluated adequately.

The remainder of this paper is organized as follows: Firstly, the basic structure of PEMFC is introduced, followed by a detailed description of its subsystems. Then, the supply system modeling is described. Secondly, the evaluation criteria are summarized, and both the design and performance of several groups of control methods are discussed. The methodology section provides a comprehensive summary and analysis of these control methods. Finally, the paper presents recommendations and perspectives for future research on PEMFCs.

2. Filtering Rules for Reviewed Articles

To ensure a high-quality and relevant literature review, the following filtering rules were applied to select the reviewed articles:

(i) Publication Date: Only articles published within the last ten years (2013–2024) were considered to ensure the inclusion of the most recent advancements in the field. The selected articles were based on three databases: ScienceDirect, Web of Science, and Google Scholar.

(ii) Research Focus: Articles specifically focusing on PEMFC supply system modeling and control strategies were selected to maintain a targeted scope.

(iii) Methodological Rigor: Studies employing rigorous methodologies and providing comprehensive data analysis were prioritized.

(iv) Citations and Influence: Highly cited articles were given preference as indicators of their impact and contribution to the field.

These filtering rules ensured the inclusion of high-quality, relevant, and recent studies, providing a solid foundation for this comprehensive review.

3. PEMFC Structure and Principles of Operation

As shown in Figure 1b, the basic structure of a PEMFC typically includes the following components: a proton exchange membrane (PEM), a catalytic layer (CL), a gas diffusion layer (GDL), and bipolar plates (BP) [41,42].

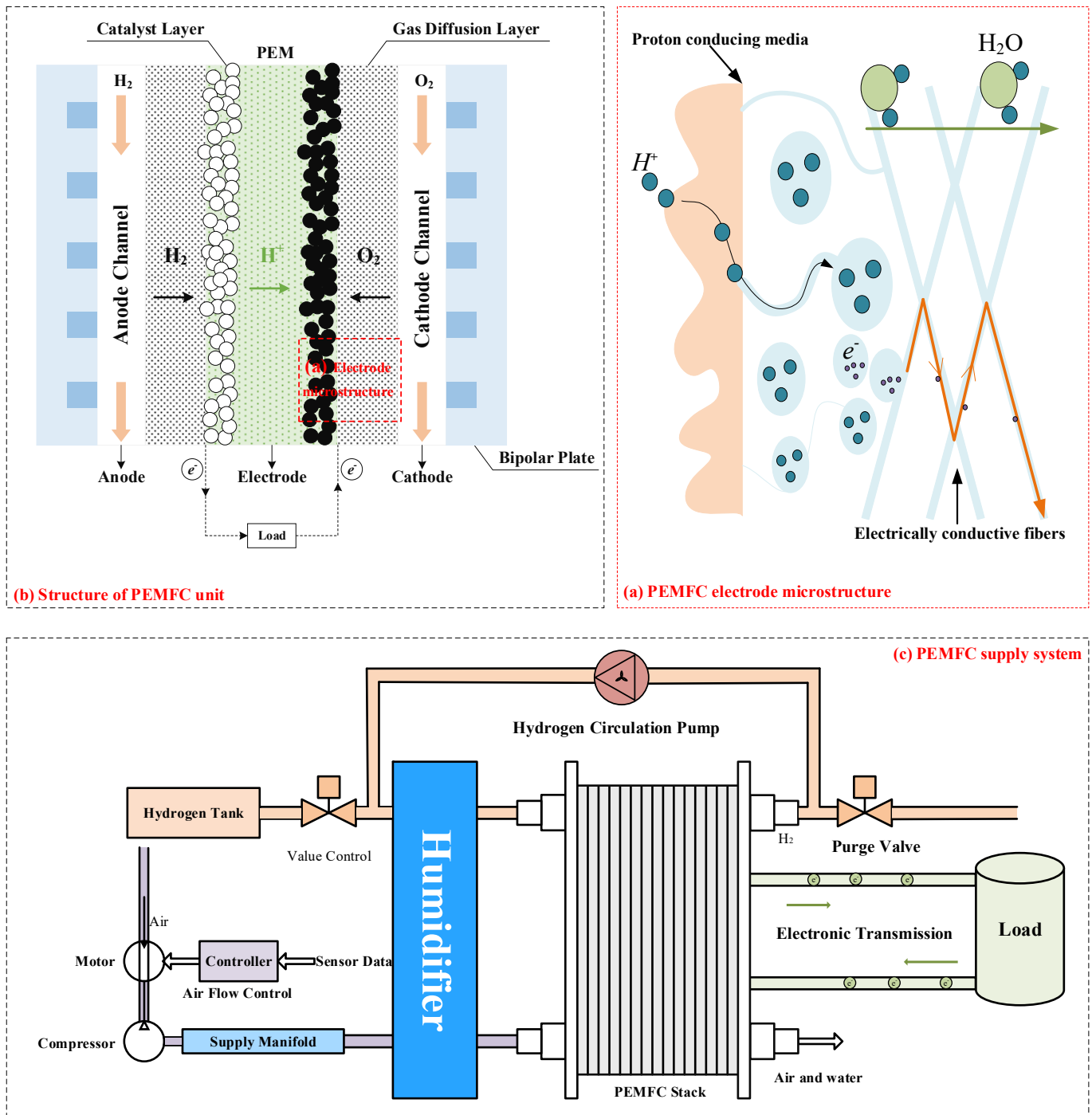


Figure 1. Structure of PEMFC.

PEM: Located at the center of the fuel cell. It is a special polymer film that allows protons to pass through while preventing the passage of electrons and other gases.

CL: Positioned on both sides of the proton exchange membrane. It consists of both the anodic catalytic layer and cathodic catalytic layer.

GDL: Located on the outer side of the catalytic layer, the GDL helps to evenly distribute the reaction gases to the catalytic layer and to export the generated water.

BP: Positioned on the outermost side of the fuel cell.

Meanwhile, Thermodynamic relationships within the PEMFC encompass reaction enthalpy, entropy, and temperature effects, dictating energy conversion efficiency, reaction spontaneity via Gibbs free energy change, and thermal management. Electrochemistry, on the other hand, focuses on charge transfer, electrode reaction kinetics, and electric potential generation, determining cell performance, efficiency, and lifespan. In PEMFCs, thermodynamics and electrochemistry interact, influencing energy conversion, reaction rate, electrode potential, and system stability.

The Nernst equation serves as a bridge between these two fields, elucidating the quantitative relationship between electrode potential and changes in reactant activity and Gibbs free energy. This equation is crucial for understanding and controlling redox reactions and electrochemical equilibrium. In the next sub-section, the PEMFC voltage model will be discussed further.

A complete PEMFC stack consists of several single-cell units connected in series to increase the output voltage and power [43]. The process is as follows: firstly, hydrogen (H_2) is decomposed into protons (H^+) and electrons (e^-) at the anode side [44]. Then, the protons reach the cathode through the PEM, while the electrons travel to the cathode through an external circuit, forming an electric current. At the cathode side, the protons, electrons, and oxygen (O_2) react to form water (H_2O), as shown in Figure 1a [45,46].

4. Modeling of PEMFC Supply System

The PEMFC system is a complex, multi-component system comprising subsystems, such as the supply system, reactor system, and thermal management system. These subsystems collaboratively ensure efficient energy conversion and precise control of the overall system [47]. Specifically, the supply system is responsible for providing and regulating the fuel and oxidizer supply. The reactor system conducts the electrochemical reactions. The thermal management system ensures the system operates within an optimal temperature range, which is essential to maintain efficiency and stability [48].

In this review, we focus on the performance of the supply systems. For the anode supply system, we ensure that the air supply is adequate with ideal humidity, and proper temperature. For the cathode supply system, it is crucial to ensure sufficient compressed hydrogen, ideal humidity, and proper temperature before the gas enters the stack. Achieving these conditions is crucial as they minimize the influence of other variables on the air supply process, thereby ensuring the accuracy and reliability of the experimental results. By eliminating the interference of external factors, the design and performance of the supply systems would be accurately evaluated and optimized. This could provide a scientific basis and technical support for future improvements to the PEMFC system [49,50].

4.1. PEMFC Stack Model

Nernst-Electric potential: The Nernst electric potential describes the change in electric potential within the fuel cell electrodes during the reaction proceeds. According to the Nernst equation, the theoretical output voltage of a single cell can be obtained as

$$E_{\text{Nernst}} = 1.229 - a(T_{\text{st}} - 298.15) + bT_{\text{st}} \left[\ln(P_{H_2}) + \frac{1}{2} \ln(P_{O_2}) \right] \quad (1)$$

where a and b are constant, P_{H_2} is the hydrogen partial pressure, P_{O_2} is the oxygen partial pressure, and T_{st} is the stack temperature.

Activation polarization overpotential: The activation polarization overpotential is a key parameter in fuel cells that describes the voltage loss due to the activation energy of the electrochemical reaction. This overpotential is usually evident at the initial stage of the

cell reaction and reflects the sluggish reaction kinetics at the electrode surface [51]. The magnitude of the activation is related to factors, such as, electrode material, electrolyte, reactant concentration, and temperature. Increasing the catalytic activity of the electrode, increasing the concentration of reactants, or raising the operating temperature typically reduces the activation overpotential. Thereby improving the performance of the fuel cell. The equation can be expressed as

$$V_{act} = -[\ell_1 + \ell_2 T_{st} + \ell_3 T_{st} \ln(C_{O_2}) + \ell_4 T_{st} \ln I_{st}] \quad (2)$$

where $\ell_1 = -0.514$, $\ell_2 = 2.86 \times 10^{-3} + 2 \times 10^{-4} \ln(A) + 4.35 \times 10^{-5} \ln(C_{H_2})$, $\ell_3 = 7.4 \times 10^{-5}$, $\ell_4 = -1.87 \times 10^{-4}$, I_{st} is the stack current. A is the activated area of the PEM, CO_2 and CH_2 are calculated by the Herry Theorem ($C_{H_2} = P_{H_2} / [1.09 \times 10^6 \exp(77/T_{st})]$ and $C_{O_2} = [P_{O_2} / 5.08 \times 10^6 \exp(-498/T_{st})]$).

Ohmic Polarization Overpotential: The Ohmic Polarization Overpotential describes the voltage loss due to the internal resistance of the fuel cell. It includes the resistance of the electrode material, electrolyte, and various connecting components. The Ohmic polarization overpotential typically increases linearly with increasing current density and can be described as

$$V_{ohm} = I_{st}(R_C + R_M) \quad (3)$$

where R_C and R_M are the equivalent resistances of the electron and proton channels, respectively.

Concentration polarization overpotential: The concentration polarization overpotential describes the voltage loss caused by the concentration gradients of the reactants and products at the electrode surfaces [52]. This overpotential arises due to the limitations in mass transport, where the rate of diffusion of reactants to the electrode surface and the removal of products away from it cannot keep up with the electrochemical reaction rates. The concentration polarization overpotential becomes more significant at high current densities and can be expressed as

$$V_{con} = m \exp(ni) \quad (4)$$

where n is the empirical value, m can be evaluated by

$$m = 1.1 \times 10^{-4} - 1.2 \times 10^{-6}(T_{st} - 273.15), T_{st} > 312.15 \text{ K}$$

$$m = 3.3 \times 10^{-3} - 8.2 \times 10^{-5}(T_{st} - 273.15), T_{st} < 312.15 \text{ K}$$

Stack output voltage and power: The actual output voltage V_C of a single cell can be expressed as

$$V_C = E_{nemst} - V_{act} - V_{ohm} - V_{con} \quad (5)$$

The stack consists of n single cells connected in series. Then, the output voltage V_{st} of stack is

$$V_{st} = nV_C \quad (6)$$

Assuming that the energy of hydrogen is completely converted into electrical energy, the theoretical fuel cell electric potential is 1.25 V [53,54]. The efficiency of the fuel cell (η) can be calculated by dividing the actual output voltage of the cell by this theoretical value [55,56]. The formula for the fuel cell efficiency is given by

$$\eta = \frac{V_C}{1.25} \times 100\% \quad (7)$$

Then, the output power P_{st} of the stack is calculated as

$$P_{st} = I_{st} V_{st} \quad (8)$$

4.2. Anode Supply System Model

As depicted in Figure 1c, the anode supply manifold is situated between the solenoid valve and the stacked anode. Gas flows from the solenoid valve and hydrogen circulation pump into the anode supply manifold and, subsequently, into the hydrogen circulation pump [57,58]. Meanwhile, the anode return manifold is positioned between the anode and the purge valve. In the relevant research, to minimize extraneous impacts on the anode supply control, the following assumptions of anode modeling were made:

- (1) All gases are ideal.
- (2) Operating temperatures of key components (valve, ejector, pump, valve) are constant.
- (3) Components function normally, ignoring vibration effects.
- (4) Hydrogen gas is fully humidified (100% relative humidity).
- (5) Nitrogen permeation from cathode to anode is negligible, and accumulated nitrogen is purged periodically.
- (6) Gas flow kinetic energy is ignored; the system is thermally isolated, and flow rates are subsonic.

The PEMFC anode undergoes electrochemical reactions by consuming hydrogen [59,60]. This process involves complex mass transfer phenomena and significantly affect the changes in gas partial pressure at the anodic reacting zone [61,62].

To simplify the calculation, let

$$\begin{cases} \frac{RT_{\text{manifold}}}{V_{\text{sm}}} = \alpha \\ \frac{RT_{\text{st}}}{V_{\text{an}}} = \beta \\ \frac{RT_{\text{m}}}{V_{\text{rm}}} = \varepsilon \end{cases} \quad (9)$$

where V_{sm} , V_{anode} , and V_{rm} represent the volumes of the anode supply manifold, anode, and return manifold, respectively. T_{manifold} is the gas temperature in the supply manifold and T_{st} is the local temperature within the anode. R is the gas constant.

Then, the anode supply system model can be described as [63,64]

$$\begin{cases} \frac{dP_{\text{sm},\text{H}_2}}{dt} = \alpha \left(\frac{dn_{\text{valve},\text{H}_2}}{dt} + \frac{dn_{\text{hcp},\text{H}_2}}{dt} - \frac{dn_{\text{smout},\text{H}_2}}{dt} \right) \\ \frac{dP_{\text{anode},\text{H}_2}}{dt} = \beta \left(\frac{dn_{\text{smout},\text{H}_2}}{dt} - \frac{dn_{\text{react},\text{H}_2}}{dt} - \frac{dn_{\text{pe},\text{H}_2}}{dt} - \frac{dn_{\text{anodeout},\text{H}_2}}{dt} \right) \\ \frac{dP_{\text{rm},\text{H}_2}}{dt} = \varepsilon \left(\frac{dn_{\text{anodeout},\text{H}_2}}{dt} - \frac{dn_{\text{hcp},\text{H}_2}}{dt} - \frac{dn_{\text{purge},\text{H}_2}}{dt} \right) \\ \frac{dP_{\text{sm},\text{vapor}}}{dt} = \alpha \left(\frac{dn_{\text{hcp},\text{vapor}}}{dt} - \frac{dn_{\text{smout},\text{vapor}}}{dt} \right) \\ \frac{dP_{\text{anode},\text{vapor}}}{dt} = \beta \left(\frac{dn_{\text{smout},\text{vapor}}}{dt} - \frac{dn_{\text{pe},\text{vapor}}}{dt} - \frac{dn_{\text{anodeout},\text{vapor}}}{dt} - \frac{dn_{\text{purge},\text{vapor}}}{dt} \right) \\ \frac{dP_{\text{rm},\text{vapor}}}{dt} = \varepsilon \left(\frac{dn_{\text{anodeout},\text{vapor}}}{dt} - \frac{dn_{\text{hcp},\text{vapor}}}{dt} \right) \\ \frac{dP_{\text{sm},\text{N}_2}}{dt} = \alpha \left(\frac{dn_{\text{hcp},\text{N}_2}}{dt} - \frac{dn_{\text{smout},\text{N}_2}}{dt} \right) \\ \frac{dP_{\text{anode},\text{N}_2}}{dt} = \beta \left(\frac{dn_{\text{smout},\text{N}_2}}{dt} - \frac{dn_{\text{pe},\text{N}_2}}{dt} - \frac{dn_{\text{anodeout},\text{N}_2}}{dt} \right) \\ \frac{dP_{\text{rm},\text{N}_2}}{dt} = \varepsilon \left(\frac{dn_{\text{anodeout},\text{N}_2}}{dt} - \frac{dn_{\text{hcp},\text{N}_2}}{dt} - \frac{dn_{\text{purge},\text{N}_2}}{dt} \right) \end{cases} \quad (10)$$

where P_{sm,H_2} , $P_{\text{anode},\text{H}_2}$, and P_{rm,H_2} are the pressures of hydrogen in the supply manifold, anode, and return manifold, respectively. Similarly, P_{sm,N_2} , $P_{\text{anode},\text{N}_2}$, and P_{rm,N_2} denote the pressures of nitrogen in the supply manifold, anode, and return manifold, respectively. $\frac{dn_{\text{valve},\text{H}_2}}{dt}$, $\frac{dn_{\text{hcp},\text{H}_2}}{dt}$, $\frac{dn_{\text{smout},\text{H}_2}}{dt}$, $\frac{dn_{\text{react},\text{H}_2}}{dt}$, $\frac{dn_{\text{anodeout},\text{H}_2}}{dt}$, $\frac{dn_{\text{purge},\text{H}_2}}{dt}$, and $\frac{dn_{\text{pe},\text{H}_2}}{dt}$ represent the molar flow rates of hydrogen in the valve, hydrogen flowing into the supply manifold from the hydrogen circulation pump, hydrogen flowing into the anode from the supply manifold, hydrogen consumed in the electrochemical reaction, hydrogen at the anode outlet, hydrogen permeating from the anode to the cathode, and hydrogen discharged from the purge valve, respectively [65]. Similarly, $\frac{dn_{\text{hcp},\text{vapor}}}{dt}$, $\frac{dn_{\text{smout},\text{vapor}}}{dt}$, $\frac{dn_{\text{pe},\text{vapor}}}{dt}$, $\frac{dn_{\text{anodeout},\text{vapor}}}{dt}$, $\frac{dn_{\text{purge},\text{vapor}}}{dt}$ and $\frac{dn_{\text{hcp},\text{N}_2}}{dt}$, $\frac{dn_{\text{smout},\text{N}_2}}{dt}$, $\frac{dn_{\text{pe},\text{N}_2}}{dt}$, $\frac{dn_{\text{anodeout},\text{N}_2}}{dt}$, and $\frac{dn_{\text{purge},\text{N}_2}}{dt}$ are the molar flow rates of vapor and nitrogen flowing into the supply manifold from the hydrogen circulation pump, flowing

into the anode from the supply manifold, permeating from the anode to the cathode, at the anode outlet, and discharged from the purge valve, respectively [66].

The hydrogen pump can be described as [67]

$$\frac{dw_{hcp}}{dt} = J_{hcp}^{-1} [c_1(u_{hcp} - c_2 w_{hcp}) - \frac{c_3}{w_{hcp}} \left(\left(\frac{P_{sm}}{P_{rm}} \right)^{\frac{k-1}{k}} - 1 \right) W_{hcp}] \quad (11)$$

where J_{hcp} represents the rotational inertia of the motor, u_{hcp} is the control voltage of the hydrogen circulation pump, and w_{hcp} is the output mass flow rate of the hydrogen circulation pump. c_x ($x = 1, 2, 3$) are the motor parameters.

Then, the state equation of anode supply system could be defined as [63]

$$\begin{cases} \frac{dx}{dt} = f(x, u) \\ y = [P_{sm}, \lambda_{hydrogen}] \end{cases} \quad (12)$$

where

$$\begin{cases} \frac{dx}{dt} = \left[\frac{dx_1}{dt}, \dots, \frac{dx_{10}}{dt} \right]^T = \left[\frac{dw_{hcp}}{dt}, \frac{dP_{sm,H_2}}{dt}, \frac{dP_{anode,H_2}}{dt}, \frac{dP_{rm,H_2}}{dt}, \right. \\ \left. \frac{dP_{sm,vapor}}{dt}, \frac{dP_{anode,vapor}}{dt}, \frac{dP_{rm,vapor}}{dt}, \frac{dP_{sm,N_2}}{dt}, \frac{dP_{anode,N_2}}{dt}, \frac{dP_{rm,N_2}}{dt} \right]^T \\ y = [x_2 + x_3 + x_4, \frac{dn_{smout,H_2}}{dn_{react,H_2}}] \\ u = [u_{valve}, u_{hcp}]^T \end{cases} \quad (13)$$

In anode control research of PEMFCs, the hydrogen excess ratio is set as a hydrogen content index, which is defined as the ratio of the supplied hydrogen flow to the actual required hydrogen flow [68]. This ratio ensures sufficient hydrogen is available for the reaction, thereby enhancing cell efficiency and managing heat and water production. Typical hydrogen excess ratio ranges from 1.2 to 2, balancing performance optimization and economic efficiency [69,70].

4.3. Cathode Supply System Model

In the cathode gas circuit, air is drawn into the supply line through a compressor firstly and humidified before being passed to the PEMFC cathode. Excess air is produced electrochemically, and water is removed via the cathode outlet [71].

Meanwhile, to simplify the influence of other factors on the air supply, the hydrodynamic systems cited model is almost assumed as follows:

- (1) All gases follow the ideal gas law.
- (2) PEMFC's thermal subsystem maintains stack temp. at 65–80 °C.
- (3) The PEMFC model is a 1D lumped parameter.
- (4) Air's $N_2:O_2$ ratio is 79:21.
- (5) Intake air relative humidity is constant and ideal.

According to the nine-state quantity model, a simplified model of a state equation with four state parameters was usually adopted in control researches of the PEMFC cathode [72]. The air management system similarly is depicted in Figure 1c. The fourth-order nonlinear state equations can be described as [73]

$$\begin{cases} \frac{dP_{O_2}}{dt} = \frac{RT_{st}k_{ca,in}}{M_{O_2}V_{ca}} \left(\frac{\lambda_{O_2,atm}}{1+\omega_{atm}} \right) (P_{sm} - P_{O_2} - P_{N_2} - P_{sat}) - \frac{RT_{st}\omega(t)}{V_{ca}} \frac{P_{O_2}}{M_{O_2}P_{O_2} + M_{N_2}P_{N_2} + M_V P_{sat}} - \frac{RT_{st}I_{st}n}{4FV_{ca}} \\ \frac{dP_{N_2}}{dt} = \frac{RT_{st}k_{ca,in}}{M_{N_2}V_{ca}} \left(\frac{1-\lambda_{O_2,atm}}{1+\omega_{atm}} \right) (P_{sm} - P_{O_2} - P_{N_2} - P_{sat}) - \frac{RT_{st}\omega(t)}{V_{ca}} \frac{P_{N_2}}{M_{O_2}P_{O_2} + M_{N_2}P_{N_2} + M_V P_{sat}} - \frac{RT_{st}I_{st}n}{4FV_{ca}} \\ \frac{dn_{motor}}{dt} = -\frac{k_t k_v \eta_{cm}}{R_{cm} J_{cp}} n_{motor} - \left(\left(\frac{P_{sm}}{P_{atm}} \right)^{\frac{\gamma-1}{\gamma}} - 1 \right) \frac{1}{n_{motor}} \frac{T_{atm} C_p}{J_{cp} \eta_{cp}} \omega_{cp} + \frac{k_t \eta_{cm}}{R_{cm} J_{cp}} u \\ \frac{dP_{sm}}{dt} = \frac{RT_{atm}\gamma}{M_{atm}V_{sm}} \left(1 + \left(\frac{1}{\eta_{cp}} \left(\frac{P_{sm}}{P_{atm}} \right)^{\frac{\gamma-1}{\gamma}} - 1 \right) \right) (\omega_{cp} - k_{ca,in} (P_{sm} - P_{O_2} - P_{N_2} - P_{sat})) \end{cases} \quad (14)$$

where u is the compressor control input. P_{O_2} is the cathode oxygen pressure, P_{N_2} is the cathode nitrogen pressure, P_{sm} represents the cathode supply manifold pressure, n_{motor} denotes the rotation speed of air compressor, and P_{sat} is the saturation pressure. Meanwhile, k_t , k_v , η_{cm} , J_{cp} , and R_{cm} are the compressor relevant parameters; $k_{ca,in}$ is the cathode inlet

orifice constant; V_{sm} and V_{ca} depict volumes of the cathode supply manifold and cathode, respectively; γ represents the ratio of specific heat of air; and P_{atm} and M_{atm} denote atmospheric pressure and air molar mass, respectively. ω_{cp} is the compressor model, and in some research, it can be described as

$$\begin{cases} \frac{dn_{motor}}{dt} = \frac{\eta_{cm}k_tk_v}{J_{cp}R_{cm}}n_{motor} - \frac{C_pT_{atm}}{J_{cp}\eta_{cp}n_{motor}}\left(\left(\frac{M_{a,atm}V_{sm}P_{sm}}{RT_{atm}\gamma}\right)^{\frac{\gamma-1}{\gamma}} - 1\right)\omega_{cp} + \frac{\eta_{cm}k_t}{J_{cp}R_{cm}}u_{cp} \\ \omega_{cp} = \frac{\omega_{cp}^{max}n_{motor}}{n_{motor}^{max}}\left(1 - \exp\left(\frac{-r(s + \frac{n_{motor}^2}{q} - P_{sm})}{s + \frac{n_{motor}^2}{q} - P_{sm}^{min}}\right)\right) \end{cases} \quad (15)$$

where s, r, q are the motor of compressor parameters.

Based on these, the cathode supply system can be depicted as

$$\begin{cases} \frac{dx}{dt} = f(x, u) \\ y = \lambda_{oxygen} \end{cases} \quad (16)$$

where

$$\begin{cases} \frac{dx}{dt} = \left[\frac{dx_1}{dt}, \dots, \frac{dx_4}{dt}\right]^T = \left[\frac{dP_{O_2}}{dt}, \frac{dP_{N_2}}{dt}, \frac{dn_{motor}}{dt}, \frac{dP_{sm}}{dt}\right] \\ y = \left[\frac{dn_{smout, O_2}}{dn_{react, O_2}}\right] \end{cases} \quad (17)$$

The oxygen excess ratio (OER) is defined as an index to evaluate oxygen content in PEMFC cathode, which is the ratio of the incoming oxygen flow to the actual oxygen flow consumed [74]. Insufficient oxygen supply will lead to extremely high concentration polarization and oxygen starvation. Long-term oxygen starvation will seriously decline the reliability and life of the PEMFC stack. Thus, inject excessive oxygen or air is required.

$$\lambda_{oxygen} = \frac{Q_{m, air, provide}}{Q_{m, air}} \quad (18)$$

5. Evaluation Criteria

The evaluation criteria of each control approach are given as follows:

- (a) Control scheme complexity: The complexity of the control scheme is evaluated based on the design and structure of the controller. This includes Classical control, Modern control, Optimized classical control and modern control, Combined controllers in series and parallel configurations. The complexity is categorized into five levels:
 - (i) Classical PID control;
 - (ii) Standard modern control or optimized classical control;
 - (iii) Optimized modern control;
 - (iv) Combined controllers or modern controller with an observer;
 - (v) Optimized modern controller with an observer.
- (b) Controller performance: The performance of the controller is assessed through key parameters including maximum error, average error, rise time, peak time, response speed, overshoot, robustness, stability, and energy consumption. These parameters are distilled into five dimensions: Error, Response speed, Overshoot, Startup time, Energy consumption. Each dimension is rated on a scale from 1 to 5 (1 for Lowest performance, 2 for Low performance, 3 for middle performance, 4 for high performance, 5 for highest performance).
- (c) Application: The application criteria include providing specific application scenarios and experimental setups as references. Each dimension and criterion are evaluated to give a comprehensive view of the control approach's effectiveness, efficiency, and suitability for various applications.

6. Cathode Control Menologies

When assessing external loads or fluctuations in PEMFCs, researchers typically adopt step currents as the disturbance input for the supply system. To establish a relationship between the oxygen flow rate provided by the air compressor and the oxygen demand for the PEMFC's optimal output, the OER has been introduced. This ratio serves as an indicator of the oxygen content within the stack relative to the optimal output power. By analyzing the correlation between OER and stack output power across various currents, researchers have derived a mathematical relationship between OER and current at the stack's optimal output power. Then, this is subsequently employed as the reference operation strategy for the controller. Based on these, the researchers determined the control framework of oxygen flow rate in the air supply system. When the current of the stack changes, the input oxygen flow rate is changed by controlling the voltage of the compressor motor, as shown in Figure 2a. Then, the actual OER always follows the ideal OER so that the oxygen content in the stack is maintained at the optimal condition for electrochemical reactions.

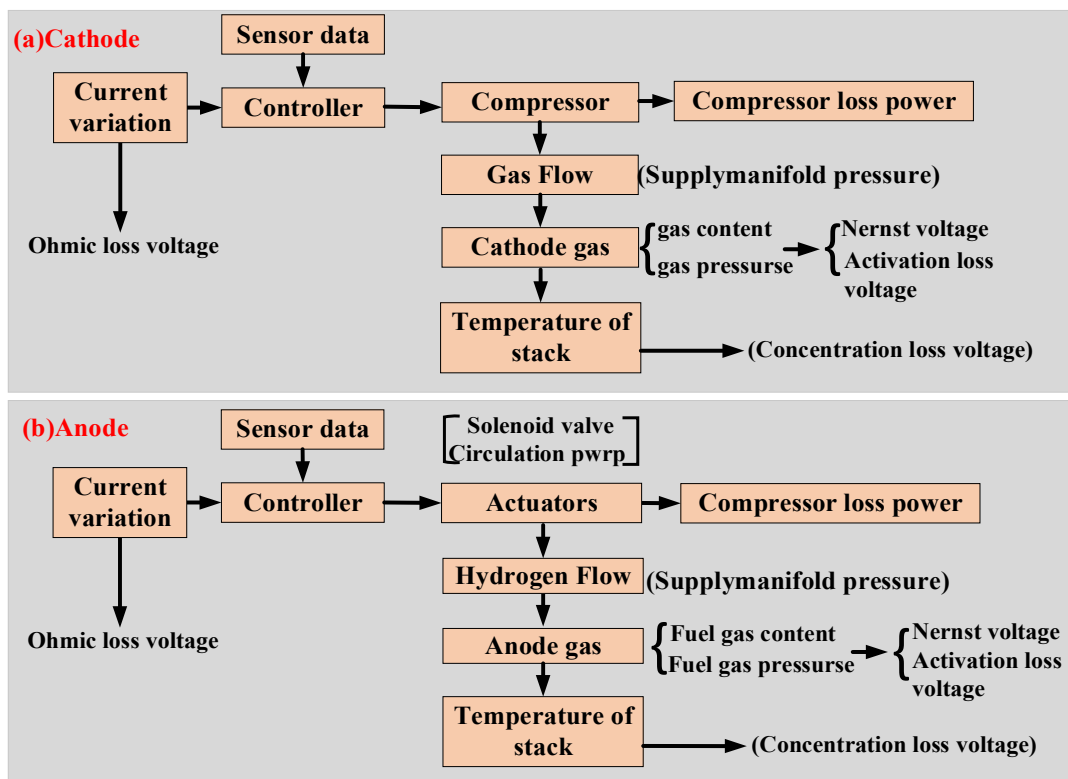


Figure 2. Principles and control structure for PEMFC supply system.

In this section, we present a comprehensive overview of the control and optimization algorithms employed over the past four years within the framework of cathode OER control. This synthesis encompasses classical, modern, and intelligent control theories, along with their respective optimization algorithms and fault-tolerance mechanisms. Our objective is to offer an exhaustive guide for future researchers in this field.

6.1. PID Control

PID control (Proportional–Integral–Derivative control) is a simple, widely used, and stable algorithm that adjusts the system output by performing proportional (P), integral (I), and derivative (D) operations on the error between the setpoint and the actual value [75]. Proportional control adjusts according to the current error, integral control adjusts according to the cumulative amount of error to eliminate steady-state errors, and differential control adjusts according to the rate of change of error to reduce overshoot and oscillation.

Therefore, the final control output is the weighted sum of these three components.

$$u(t) = K_p e + K_i \int_0^t e dt + K_d \frac{de}{dt} \tag{19}$$

where u is the control input, e is the system error, and K_p , K_i , and K_d are the gains of the proportional-integral differential terms, respectively.

However, it also has certain disadvantages, such as difficult parameter adjustment and possible high delay for nonlinear systems. In many complex operating conditions, PID [76] is generally used in combination with other control methods or algorithms [77–88].

As shown in Figure 3, we have selected five typical optimized PID control methods, (a) Particle swarm optimized PID control [86], (b) Fuzzy PID control [80], (c) Neural network PID control [81], (d) Fuzzy and neural network composite PID control [82], and (e) Fractional step PID control with an observer [83]. Case a to c corresponds to Global Optimization, Online Optimization, and Intelligent Optimization, respectively. And d and f represent Hybrid Optimization. Global optimization uses potent search algorithms to avoid local optima and fine-tunes PID parameters globally by iteratively calculating performance indices over the entire simulation. Online optimization, leveraging fuzzy logic, model reference adaptive, or self-tuning control, adjusts PID parameters in real-time based on error and its derivatives. Meanwhile, intelligent employs reinforcement learning or neural networks, developing a black-box model from training data to tune PID parameters. And hybrid integrates observers or other control techniques with PID control, adjusting parameters or combining outputs for tuning.

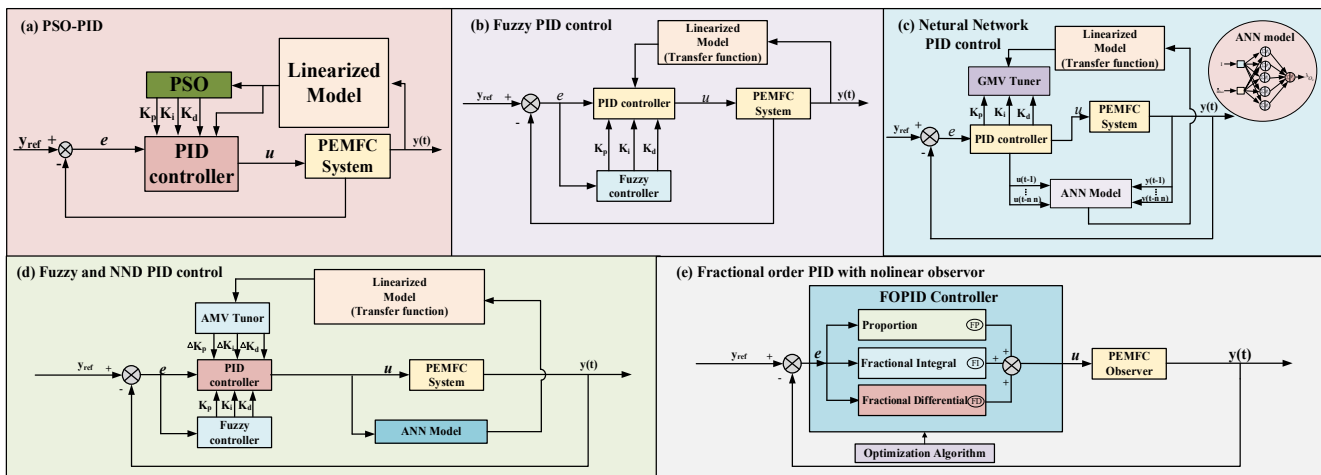


Figure 3. Optimized PID controls.

These controller performance evaluations are summarized in Figure 4 according to Appendix A. The single optimization algorithm significantly improves performance compared to the traditional PID controller in PEMFC cathode control. However, the composite algorithm offers limited improvement over single optimization algorithm. The optimized PID control method combined with an observer achieves further performance gains. Since the PID is a classical controller, performance improvements are limited unless a combination controller is used. Meanwhile, using a PID controller requires linearizing the PEMFC system.

6.2. Sliding Mode Control

Sliding Mode Control (SMC) is extensively utilized as a control strategy in various industrial and engineering settings and basic structure [89]. It is particularly valued for its robustness against changes in system parameters and external disruptions. Considering that PEMFC is coupled complex systems, SMC is more suitable than PID because of its

nonlinear characteristics. Sliding mode controllers have been prevalently applied in PEMFC systems according to past research [90,91].

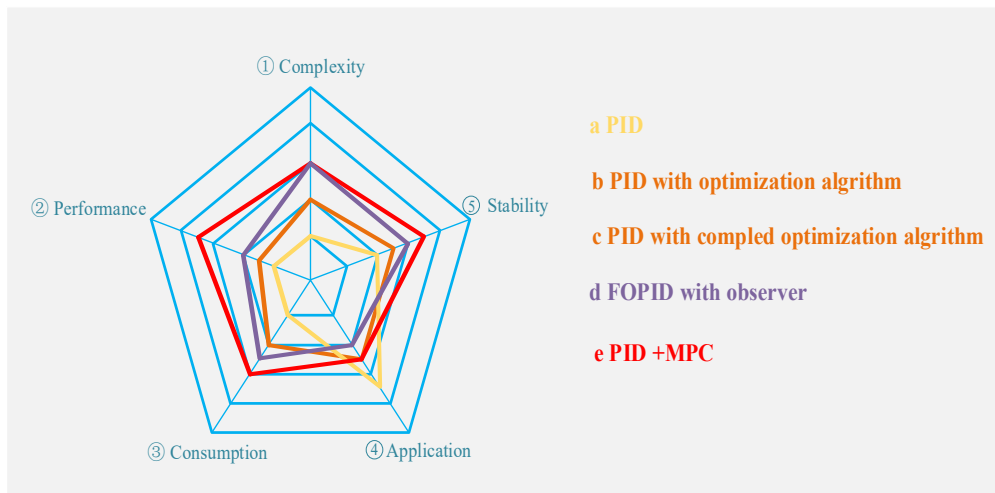


Figure 4. Overall assessments for PID series control.

In comparison to PID control, SMC presents strong robustness, excellent tracking performance and heightened system stability. However, control inputs may exhibit high-frequency oscillations upon approaching the ideal sliding surface. Based on these, terminal sliding mode structure (TSMC) utilizes a nonlinear sliding surface that facilitates quicker convergence of the system state towards the sliding surface [92,93].

Further, Non-singular terminal sliding mode control (NTSMC) was proposed to avoid the singularity issue in TSMC by redesigning the sliding mode variable, which would enhance both the response speed and robustness [94,95]. These sliding variables are shown in Table 1, where e is the system error, α and β are the sliding mode gains, respectively, p and q represent positive odd numbers, and they satisfy $1/2 < p/q < 1$, and $\lambda(e)$ can be described as

$$\lambda(e) = \begin{cases} e^{p/q} & \text{if } \hat{s} = 0 \text{ or } \hat{s} \neq 0, |e| \geq \mu \\ \gamma_1 e + \gamma_2 \text{sign}(e)e^2 & \text{if } \hat{s} \neq 0, |e| < \mu \end{cases} \quad (20)$$

where $\hat{s} = \frac{de}{dt} + \kappa_1 e + \kappa_2 e^{p/q}$, μ is a sufficiently small positive number, $\gamma_1 = (2 - p/q)\mu^{p/q-1}$ and $\gamma_2 = (p/q - 1)\mu^{p/q-2}$.

Table 1. Typical sliding variable structure.

Sliding Variable	Sliding Variable Structure
Classic nonlinear sliding mode variable	$s = \frac{de}{dt} + \alpha e$
Terminal sliding mode variable	$s = \frac{de}{dt} + \alpha e + \beta e^{p/q}$
Non-singular terminal sliding mode variable	$s = \frac{de}{dt} + \alpha e + \beta \lambda(e)$

The derivative of the sliding variable s is set to zero. Solving this equation inversely provides the control signal u . The derived control law u thus ensures that the system trajectory remains on the sliding surface.

In addition to the aforementioned structures, prevalent sliding mode configurations also encompass (i) Integral sliding mode control: the introduction of an integral term eliminates the steady state error and enhances the robustness of the system to disturbances; (ii) High-order order sliding mode control: this control strategy involves the higher order derivatives of the state, which effectively reduces the jitter [96]; and (iii) Discrete time sliding mode control: it is suitable for sampled data systems.

Meanwhile, SMC incorporates dynamically adjustable gain parameters. Through optimization techniques, sliding mode gains can be continuously updated based on real-time

performance metrics. This includes various methods such as time delay estimation algorithms [92], fault tolerance mechanisms [97,98], hierarchical optimal control strategies [99], super-twisting algorithms [100], and fuzzy algorithms [101]. Furthermore, integrating SMC with observers like the extended state observer [102,103], adaptive algebraic observer [104], and disturbance observer [105] significantly improves both performance and stability.

As shown in Figure 5, five optimized SMC structures are identified for evaluation here: (a) an optimization-based two-loop SMC [98], (b) an observer-based fault-tolerant SMC [97], (c) an adaptive SMC with optimization algorithms [100], (d) a two-loop SMC based on observations [77], and (e) NTSMC based on fuzzy logic [94].

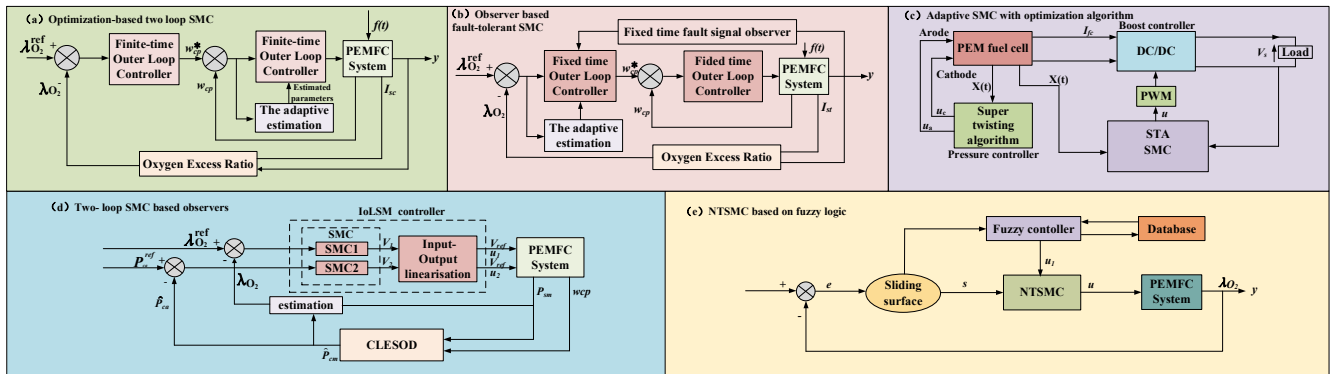


Figure 5. Optimized sliding mode controls.

These results are categorized in Figure 6 according to Appendix A. Owing to the comprehensive optimization of the sliding mode structure, NTSMC demonstrates enhanced performance and stability relative to both TSMC and SMC. However, the design of the NTSMC is relatively more complex and imposes greater demands on the actuator.

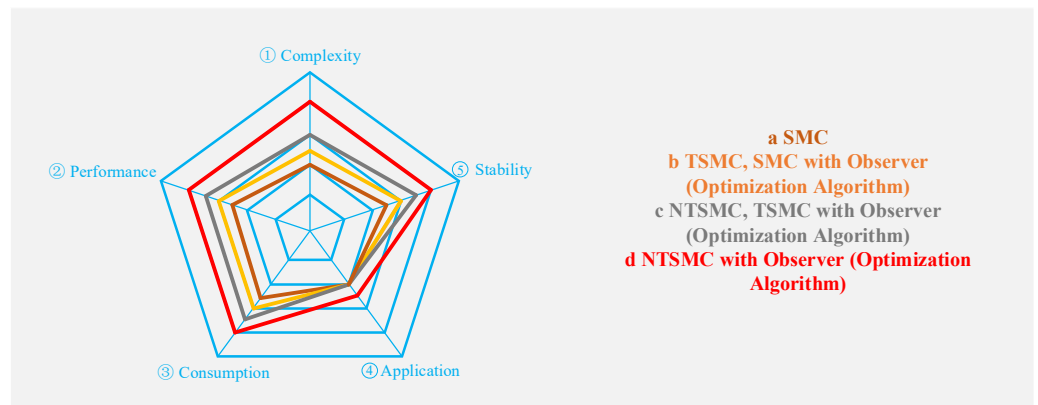


Figure 6. Overall assessments for SMC series control.

6.3. Optimal Control and Model Predict Control (MPC)

Optimal control entails devising a control strategy that optimizes a specified performance metric, which considers both the dynamics of the system and the existing constraints [106]. This performance metric is typically represented as a cost function. The primary goal of the optimal control is to minimize this cost function, thereby maximizing the associated benefit.

The fundamental principle of the MPC is to employ a mathematical model of the system to optimize control inputs based on predictions [107,108].

MPC and optimal control both aim to enhance system performance, but their applications and methodologies are distinctly focused. Optimal control primarily seeks to identify the global optimal solution throughout the operational period. In contrast, MPC addresses

the local optimization problem in each control cycle and continuously updates the control strategy to accommodate system variations and constraints.

A Linear Quadratic Regulator (LQR) is one of these optimal control methods [109] specifically designed for linear systems. Its primary objective is to minimize a specific form of quadratic performance index. However, as shown in Figure 7, application of LQR necessitates the linearization of the PEMFC supply system [88,110].

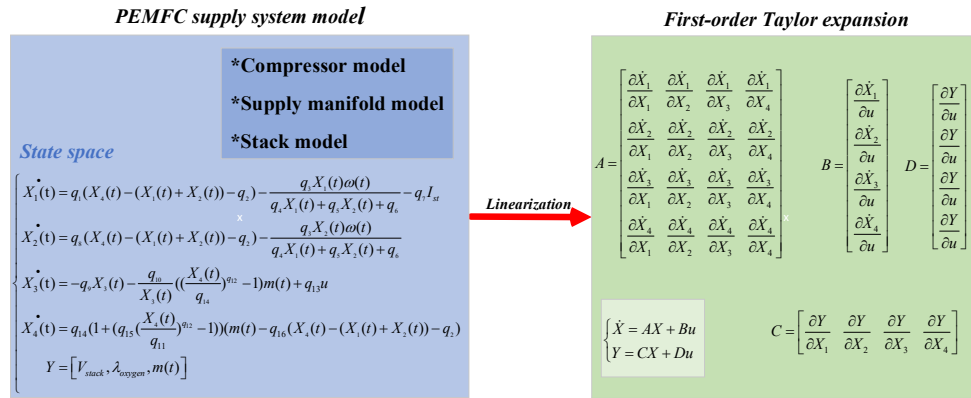


Figure 7. The linearization process for PEMFC supply system.

After linearization, the state equation of the supply system can be described as

$$\begin{cases} \frac{dX(t)}{dt} = AX(t) + Bu \\ Y = CX(t) + Du \end{cases} \quad (21)$$

where A, B, C, and D are the system matrixes that describe the system dynamics. Then, the cost function is

$$J = \int_0^\infty (X^T Q X + u^T R u) dt \quad (22)$$

where R represents weighting matrices; Q is semi-positive, while R is positive definite. Increasing Q leads the system to prioritize minimizing state error, whereas increasing R shifts the focus towards conserving control energy.

The solution to the LQR problem involves solving the algebraic Riccati equation

$$A^T P + PA - PBR^{-1}B^T P + Q = 0 \quad (23)$$

where P is a positive definite symmetric matrix. Once P is computed, the optimal control law can be expressed by

$$\begin{cases} u = -KX \\ K = R^{-1}B^T P \end{cases} \quad (24)$$

What is more, there is a near-time optimal control method that fits for the nonlinear system. According to the receding horizon optimization theory, J can be dedicated as,

$$J = \int_0^{T_f} e^T(t + \sigma) R e(t + \sigma) d\sigma \quad (25)$$

where T_f is the time domain parameter of optimization. Based on the Taylor series, it can be amplified as [111]

$$e(t + \sigma) = e + \sigma \frac{de}{dt} + 0.5\sigma^2 \frac{d^2e}{dt^2} \quad (26)$$

Then, the Taylor-expanded error is substituted to calculate the factor J, which is subsequently solved for the control variable u through a method analogous to the LQR.

MPC outperforms optimal control due to its adaptability, predictive capabilities, and constraint management [63,112]. The MPC algorithm comprises a predictive model,

feedback correction, and rolling optimization. It achieves steady state after Z time steps, where Z is the modeling time domain. The values at sampling points form the model vector. With N as the prediction horizon and M as the control horizon, the predictive output for future states can be expressed in terms of the current state [88]

$$Y = Y_0 + P\Delta u$$

$$\begin{bmatrix} Y_M(k+1|k) \\ Y_M(k+2|k) \\ Y_M(k+3|k) \\ \dots \\ Y_M(k+N|k) \end{bmatrix} = \begin{bmatrix} Y_0(k+1|k) \\ Y_0(k+2|k) \\ Y_0(k+3|k) \\ \dots \\ Y_0(k+N|k) \end{bmatrix} + \begin{bmatrix} p_1 & 0 & \dots & 0 \\ p_2 & p_1 & \dots & 0 \\ p_3 & p_2 & \dots & 0 \\ \dots & \dots & \dots & \dots \\ p_N & p_{N-1} & \dots & p_{N-M-1} \end{bmatrix} \begin{bmatrix} \Delta u \\ \Delta u(k+1) \\ \Delta u(k+2) \\ \dots \\ \Delta u(k+M-1) \end{bmatrix} \quad (27)$$

where k represents current time step, Y_0 , Y_m , Δu , and P denote the initial predict value, the predict value after M time steps, control increment, and the dynamic coefficient, respectively. This formulation indicates that the prediction for $k + N$ time step is based on the k time step.

The goal of the MPC is to minimize a cost function over the prediction horizon, and its cost function can be presented as

$$\min J = \sum_{i=0}^{N-1} a|Y_M(k+1+i)|k - \eta(k+1+i)| + \sum_{i=0}^{M-1} b|\Delta u(k+i)|^2 \quad (28)$$

In the proposed formulation, a and b represent the inhibition coefficients corresponding to the tracking errors and incremental changes, respectively, and η denotes the anticipated output. Let $\partial J / (\partial \Delta u) = 0$ and we can obtain $\Delta u(k) = f^T (P^T Q P + D)^{-1} P^T Q [\eta(k) - Y_0(k)]$, in which f is used to select the initial element for computation, Q and D serve as the error weighting matrix and control weighting matrix, respectively.

By solving this optimization problem, MPC computes a series of optimal control input u . Only the first control input (u_0) is applied initially. At the subsequent control step, the system state is updated, and the optimization problem is re-solved, thereby forming a continuous rolling optimization process [113]. The cost functions of above control methods are summarized in Table 2.

Table 2. Common cost function of optimal controls.

Optimal Control Type	Common Cost Function
LQR	$J = \int_0^\infty (X^T Q X + u^T R u) dt$
Near-time optimal control	$J = \int_0^{T_f} e^T (t + \sigma) Re(t + \sigma) d\sigma$
MPC	$J = \sum_{k=0}^{N-1} (X^T Q X + u^T R u) + X_N^T P X_N$

Both Optimal Control and MPC can be enhanced by integrating optimization algorithms or observers to achieve further performance improvements. These optimization schemes include a neural network algorithm [114], fuzzy logic algorithm [115], observers [116,117], and a series-parallel connection with PID controllers [88].

Four optimal control and MPC structures are identified for evaluation here: (a) near-time optimal control with SMO [118], (b) MPC with neural network algorithm [114], (c) MPC with observer [116], and (d) MPC with nonlinear observer [117]. Their structures and the performance evaluations are shown in Figures 8 and 9, respectively.

Among the selected control schemes, the optimal control integrated with an optimization algorithm approaches the performance of conventional MPC. However, MPC enhanced with a neural network algorithm exhibits the strongest performance according to Appendix A. For the complex and changing environment of the PEMFC, MPC has a stronger ability to adapt and adjust than optimal control.

6.4. H Index Control

Both H_∞ [119] and H_2 control are two important robust control strategies in modern control theory. These methods design control systems using different performance metrics to ensure stability and their differences are summarized in Table 3.

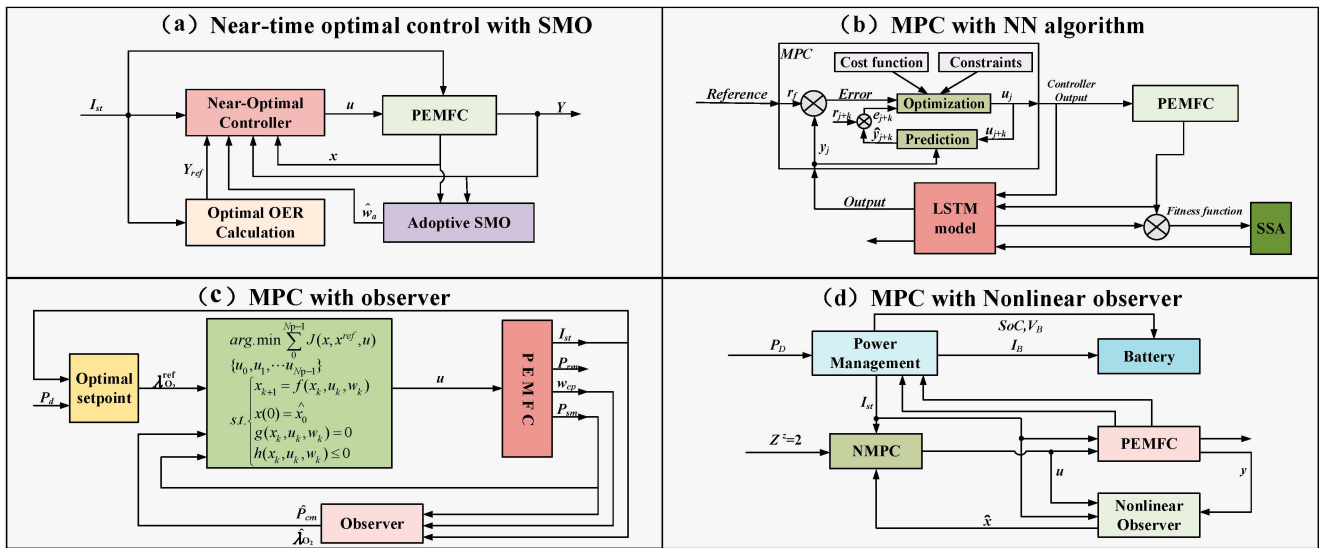


Figure 8. Optimized optimal control and MPC.

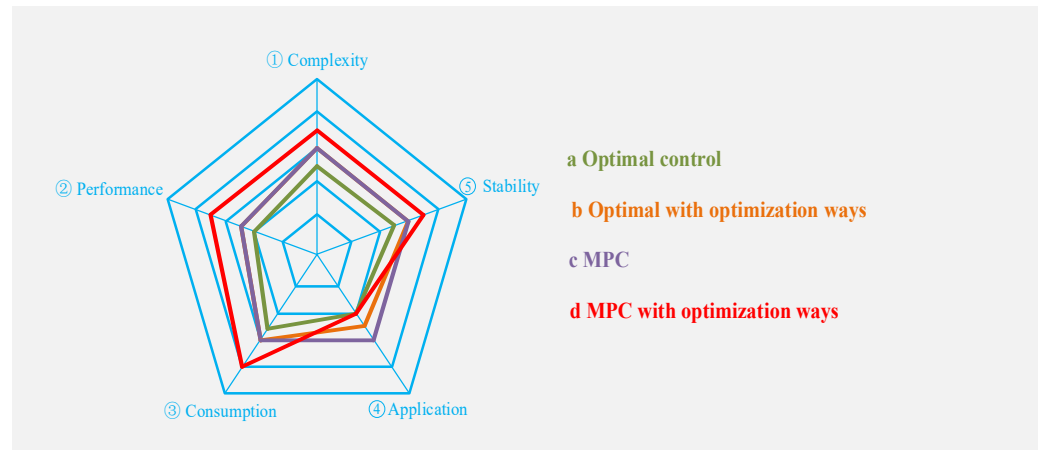


Figure 9. Overall assessments for optimal control and MPC.

Table 3. Differences between $H\infty$ and $H2$ control.

Difference	$H\infty$ Control	$H2$ Control
Performance indicator	Emphasis on worst-case system performance [120]	Focus on average system performance
Application	Extreme conditions	Disturbances are more routine
Complexity	More sophisticated	Sophisticated

The design of nonlinear $H\infty$ [121] control typically involves finding a control law ($u = k(X)$) that minimizes the worst-case performance loss (maximum $H\infty$ paradigm) of the output due to external disturbances. This is generally achieved by constructing a Hamilton–Jacobi–Isaacs (HJI) equation,

$$\min_u \max_\omega (Vf(X, u) + g(X, u)\omega + \|Y\|^2 - \gamma^2 \|\omega\|^2) = 0 \tag{29}$$

where ω are the external disturbances, V represents a Lyapunov function to be solved and γ is a predetermined performance bound. Solving the HJI equation typically requires numerical methods, such as dynamic programming or grid methods. The solution of this equation V can be used to construct the control law u . This can be accomplished using Robust Control Toolbox in MATLAB_{2012a}.

The goal of nonlinear H_2 [122] control is to design the controller to minimize the desired square integral ($\int_0^\infty Y^T Y dt$) of performance output due to the external disturbances ω . This typically involves solving a corresponding optimization problem, which may require the use of linearization methods as described previously.

Due to the characteristics of the controller structure, H_∞ control is more suitable than H_2 for PEMFC supply system. However, there have been fewer studies on related controllers in the last decade [123].

6.5. Intelligent Control

Intelligent control represents a contemporary control technique that merges principles from computational intelligence, machine learning, and traditional control theory. Intelligent control algorithms possess the capability to learn the system behavior [124], optimize the control strategy, and adapt to both unknown and evolving environments [125].

Controllers based on machine learning optimization were introduced in the previous sections [126,127]. This section focuses on pure machine learning and reinforcement learning controllers. Such controllers tend to be model-free, relying on data and samples for control.

6.5.1. Complex Fuzzy Control

Type-2 fuzzy control extends fuzzy logic to better handle uncertainty by using fuzzy sets where membership degrees are also fuzzy, unlike the deterministic memberships in Type-1 [128]. This method improves the management of system uncertainty and noise. The basic processes of Type-2 fuzzy control include the following:

- (i) Fuzzification: Converts precise inputs into fuzzy inputs (Type-2 fuzzy sets).
- (ii) Rule Base: Contains a set of fuzzy rules that define the relationship between input fuzzy sets and output fuzzy sets.
- (iii) Inference Mechanism: Uses fuzzy logic inference to evaluate the rules and generate the fuzzy outputs.
- (iv) Defuzzification: Converts the fuzzy outputs into precise outputs, typically by computing the center of gravity or another representative value of the output fuzzy set.

Type-2 fuzzy controllers are widely used in various industrial and advanced control systems due to their effectiveness in handling uncertain and complex environments. Two control schemes are chosen for evaluation here: (a) one with an observer [129] and (b) one without an observer [130], as shown in Figure 10, owing to the fact that advanced fuzzy control with an observer can better handle the nonlinear characteristics of PEMFC and perturbation under a variable current.

As can be seen from Appendix A, the Type-2 fuzzy controller does not have a performance advantage over modern control methods and places higher demands on the actuator.

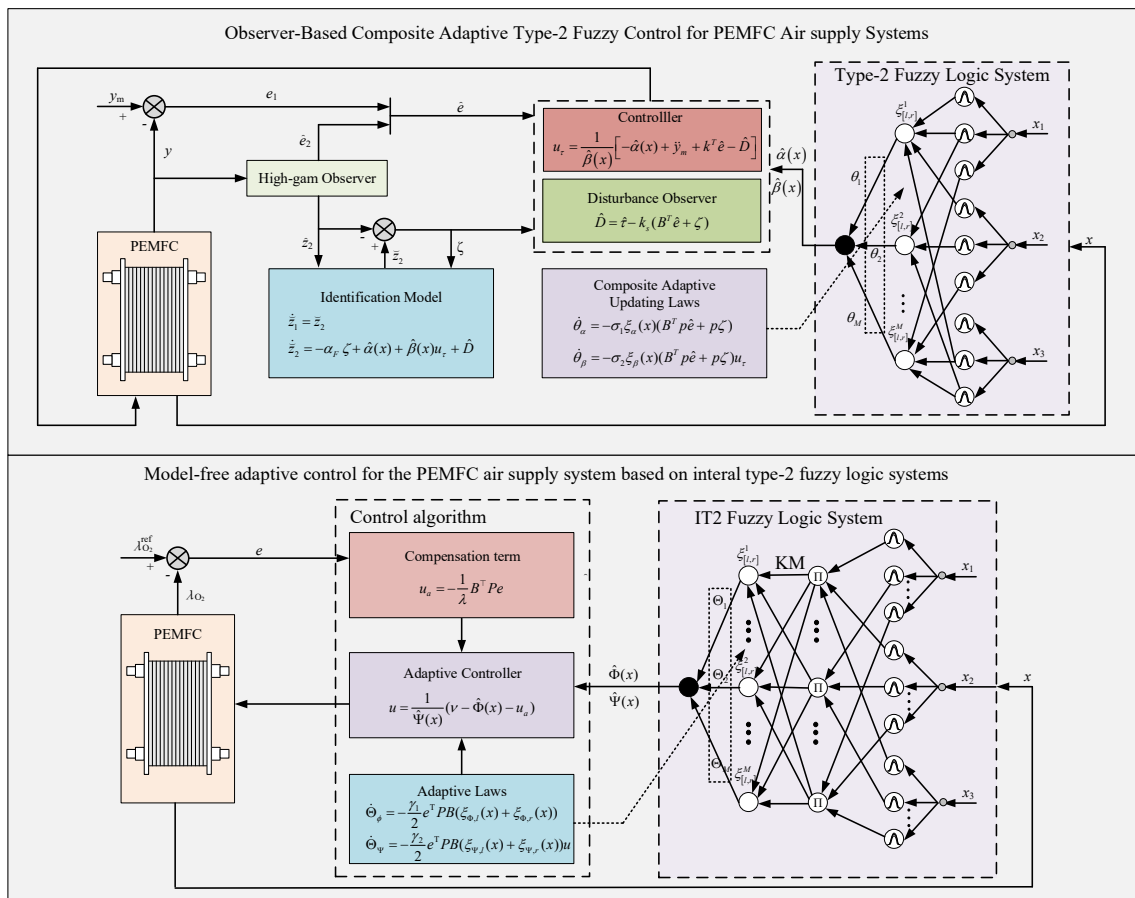


Figure 10. Structures of selected Type-2 fuzzy control approaches.

6.5.2. Direct Neural Network Control

Direct neural network control (DNC) is an approach that uses artificial neural networks to generate control signals directly without an explicit system model [131,132]. This control strategy achieves effective regulation of complex or nonlinear systems by learning the input-to-output mapping relationship through neural networks [133]. Therefore, this approach can adapt to varied operation conditions of PEMFC better. The working principle of DNC could be illustrated as follows:

- (i) **Network Structure Selection:** Choose a suitable neural network structure based on the complexity of the control task and the characteristics of the data. Common structures include feed-forward neural networks, recurrent neural networks, and convolutional neural networks.
- (ii) **Data Collection and Training:** Collect input and output data of the system under different operating conditions. These data are used to train the neural network, enabling it to learn how to generate appropriate control signals based on the current system state and external inputs.
- (iii) **Network Training:** Utilize supervised learning methods to train the neural network with the collected data. The goal of training is to minimize the error between the predicted output and the actual output.

In recent years, DNC has become a hotspot in the PEMFC supply system. Various structures have been explored, including the B-SNN-based structure [133], PPF-based structure [134], RBF-based structures [135], NARX and NOE-based structures [136], linearized and free radical neural networks [137], neural network identifying inverse models [138], neural network with backstepping [139], and neural network with observers [140,141].

Neural networks with observers (a and b) are given here as an evaluation [140,141]. Their configurations are shown in Figure 11. As depicted in Appendix A, it is not easy to see

that DNC is more powerful compared to fuzzy control. Overall, the optimized DNC could achieve performance close to that of MPC. In terms of controller design, DNC requires less computation than MPC, but it does place more demands on the actuator.

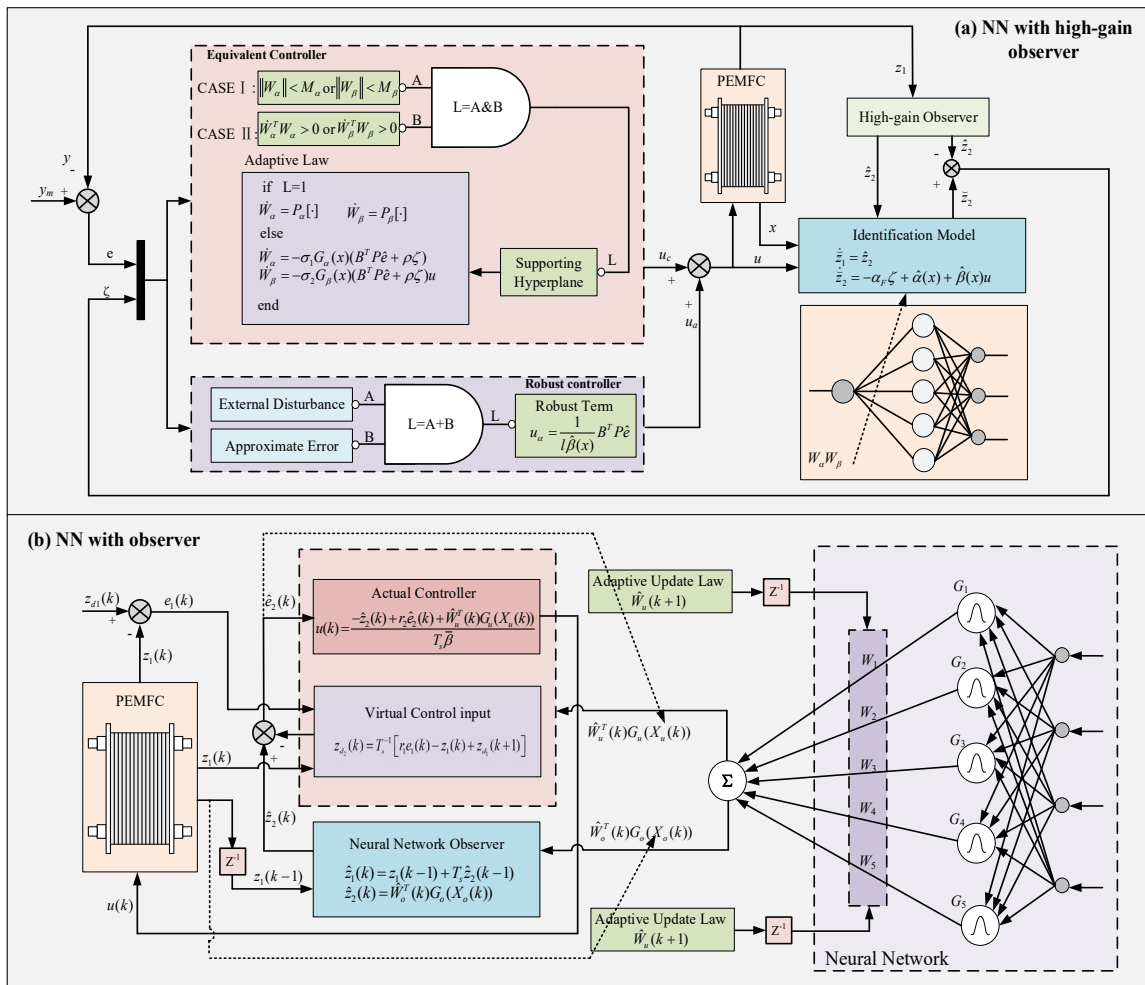


Figure 11. Structures for selected DNC approaches.

6.5.3. Deep Reinforcement Learning Direct Control

Deep Reinforcement Learning (DRL) combines the complex data processing capabilities of Deep Learning with the decision-making mechanisms of Reinforcement Learning, providing a powerful framework for direct control modeling. This approach enables intelligent agents to self-learn optimal strategies of PEMFC to maximize cumulative rewards as they interact with their environment. As shown in Table 4, current mainstream research is based on Q-learning (QL), Deep Deterministic Policy Gradient (DDPG), and Soft Actor-Critic (SAC) algorithms. Their structures are shown in Figure 12 respectively.

Table 4. Differences between QL, DDPG, and SAC.

Algorithm	Action Space	Core Strengths	Main Challenges
QL	Discrete	Easy to implement, low computational needs	Struggles with high-dimensional or continuous action spaces
DDPG	Continuous	Handles continuous action spaces, integrates deep learning	Requires substantial computational resources, potential for unstable learning
SAC	Continuous	Maximizes entropy to enhance exploration, stable and efficient learning	Complex implementation, high computational demands

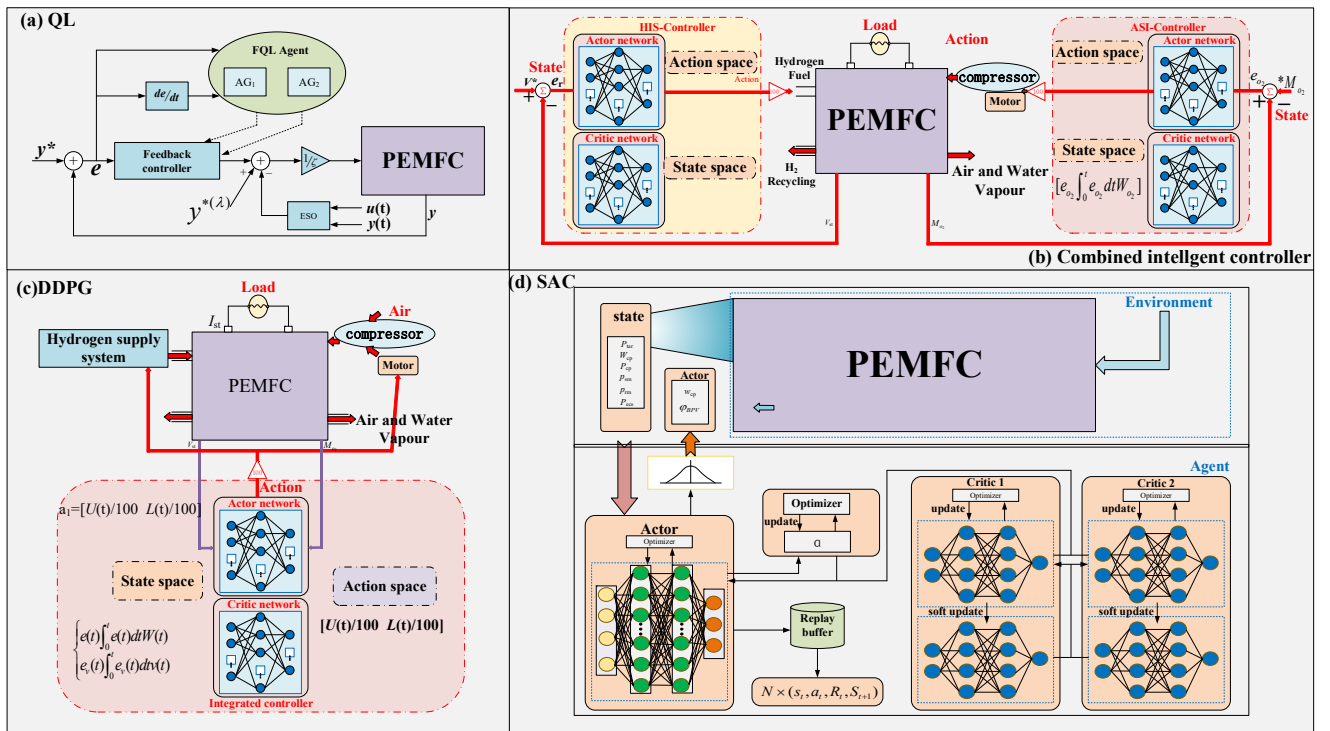


Figure 12. Structures for DRL controllers.

QL aims to learn a strategy that maximizes cumulative future rewards by guiding the agent to make optimal decisions through learning the value (Q-value) of each state-action pair. The strategy of Q-learning is usually based on the ϵ -greedy algorithm. QL maintains a Q-table, a two-dimensional table in which each element represents the value of a state-action pair. The Q-value is updated using the following formula:

$$Q\langle s, a \rangle \leftarrow Q\langle s, a \rangle + \alpha[r + \gamma \max_{a'} Q\langle s', a' \rangle - Q\langle s, a \rangle] \quad (30)$$

where s is the current state, a is the action taken in state s , r is the immediate reward received for taking action a , and s' is the next state resulting from action a . Meanwhile, α is the learning rate, which determines how quickly the new information overwrites the old, and γ is the discount factor, which determines the importance of future rewards.

DDPG is to use two main neural networks: an Actor network and a Critic network. The Actor network outputs a determined action based on the current state, and the Critic network assesses the expected payoff of this action in the current state. Several key techniques in DDPG include the following:

- (i) **Replay Buffer:** DDPG uses a replay buffer to store the state, action, reward, and next state at each step. This buffer enables random sampling during training, reducing data correlation and preventing overfitting.
- (ii) **Target Networks:** To stabilize the learning process, DDPG employs target networks for both the Actor and Critic. The parameters of these target networks slowly converge to those of the main networks, helping to stabilize the performance of the learning algorithm.
- (iii) **Exploration:** In continuous action spaces, DDPG enhances exploration by adding noise (e.g., the Ornstein–Uhlenbeck process) to the Actor's output actions, facilitating effective exploration of the environment.

SAC is a deep reinforcement learning algorithm for continuous action spaces. It is model-free, off-policy, and optimizes exploration by balancing expected return and policy entropy. It uses two critic networks to reduce overestimation and enhance robustness, with the actor network outputting optimal, diverse actions based on both return and entropy.

Critic updates incorporate rewards and future values into a soft value function. Key steps include data sampling, critic/actor updates, and dynamic entropy weight adjustment for exploration–exploitation balance.

According to the results presented in Table 5, SAC demonstrates the strongest performance, followed by DDPG, with QL performing the worst. Composite or optimized algorithmic models show the best overall performance. However, it is generally observed that deep reinforcement learning demands high actuator performance for PEMFC operation, especially in parallel computing, leading to increased energy consumption with limited improvement over modern control methods.

Table 5. Evaluations of recent relevant researches in DRL application.

Citation	Algorithmic Strategy	Performance Indexes (The Number of '★' Represents the Level of Evaluation)
[142], 2021	EILMMA-DDPG	Complexity: ★★★ Consumption: ★★★★★ Performance: ★★★★★
[143], 2020	CIED-MD3	Complexity: ★★★ Consumption: ★★★★★ Performance: ★★★★★
[144], 2021	ECMTD-DDPG	Complexity: ★★★ Consumption: ★★★★★ Performance: ★★★★★
[145], 2024	SAC	Complexity: ★★ Consumption: ★★★★★ Performance: ★★★★★
[146], 2023	MADDPG	Complexity: ★★★ Consumption: ★★★★★★ Performance: ★★★★★
[147], 2023	FO-DDPG	Complexity: ★★★ Consumption: ★★★★★★ Performance: ★★★★★★
[148], 2022	SAC	Complexity: ★★ Consumption: ★★★★★★ Performance: ★★★★★
[149], 2021	ECILS-MADDPG	Complexity: ★★★★★ Consumption: ★★★★★★ Performance: ★★★★★★
[150], 2024	MASFQL	Complexity: ★★★ Consumption: ★★★★★★ Performance: ★★★★★

As illustrated in Figure 13, controllers based on deep reinforcement learning can handle PEMFC control issues better than complex fuzzy and neural network controllers. But they require higher performance of PEMFC controller. Unlike the modern controllers discussed in the previous section, intelligent controllers do not necessitate complex computational steps.

6.6. Observer-Based Control

In control theory, an observer is an algorithm used to estimate the state of a system, particularly when the full state of the system cannot be measured directly. Through the observer, the control system can accurately calculate the disturbances of the PRMFC system in the face of sudden changes. Meanwhile, it can also predict the parameters or state coefficients that are hard to measure in the PEMFC system. Thus, it has a wide range of applications in PEMFC supply systems, including a sliding mode observer [118], neural network observer [140], high-gain observer [151], Kalman Filter [152], Luenberger observer [153], and Algebraic observer [154].

In the above sections, it is evident that the inclusion of the observer algorithm further improves the performance of the controller. However, the observer requirements vary depending on the state equations of PEMFC, and controller requirements. These specifics need to be addressed in context and are characterized as shown in Table 6.

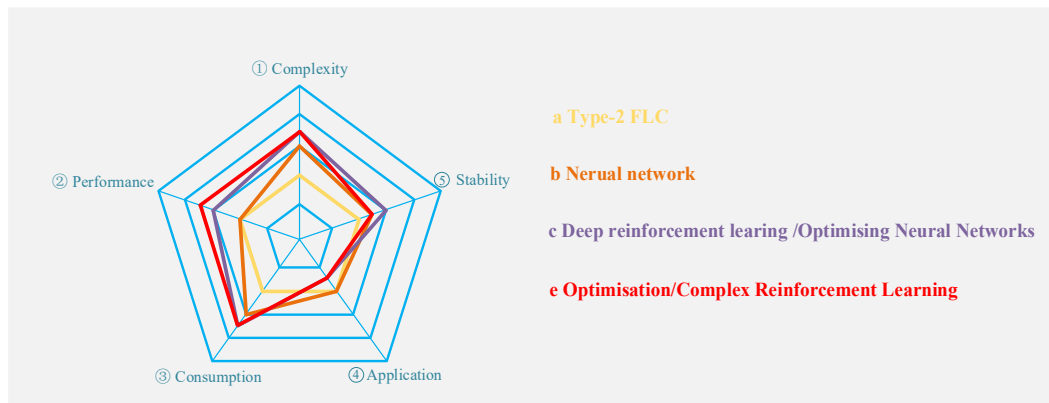


Figure 13. Overall evaluation for intelligent controllers.

Table 6. Characteristics of the observers.

Observer Type	Advantages	Disadvantages
Sliding Mode Observer, [118]	High robustness, quick response to state changes.	May produce chattering, affecting performance and life.
Neural Network Observer, [140]	Adapts to nonlinear and complex systems, handles complex pattern recognition.	Requires extensive training data, sensitive to initial conditions, time-consuming training.
High-Gain Observer, [151]	Simple implementation, tolerant to model inaccuracies.	Sensitive to noise, high gain may amplify measurement noise.
Kalman Filter, [152]	Optimal state estimation in noisy environments, especially suitable for linear systems and Gaussian noise.	Requires linearization for nonlinear systems, high computational complexity.
Luenberger Observer, [153]	Simple structure, suitable for linear systems, easy to implement.	Depends on accurate system models, low robustness to model errors and external disturbances.
Algebraic Observer, [154]	Real-time state reconstruction without needing initial states, resistant to certain disturbances.	Complex design and implementation for high-order or dynamically complex systems.

6.7. Fault-Tolerance Mechanism

Fault-tolerant control is a technique designed to ensure that a system continues to operate normally, despite the failure of some of its components [155]. The process involves fault detection, diagnosis, isolation, and recovery measures aimed at enhancing the safety, reliability, and robustness of the system [156].

Fault-tolerant control for the PEMFC supply system encompasses several key aspects: fault-tolerant control of the supply manifold [157], fault-tolerant control of the valves [158], fault-tolerant control of the compressor [159], and data-based fault-tolerant control [160]. Each component is crucial for maintaining system integrity and operational continuity under fault conditions.

Considering backpressure valve failure, it is proposed to substitute the parameter used to control the valve opening with a fault factor f_1 , followed by a reconstruction of the state equation. Additionally, considering leakage in the supply manifold, it is suggested to incorporate a leakage fault factor f_2 , to adjust the relationship between the outlet flow rate of the supply manifold and the inlet flow rate of the cathode, leading to a further reconstruction of the PEMFC state equation [158]. An observer can also be constructed for fault estimation, where faults are treated as additional state variables. By incorporating PEMFC state addition terms, an additional system is constructed, and a corresponding observer is then designed for the reconstruction of the faulty system [155,161].

Meanwhile, various fault conditions can affect the air compressor, such as overheating, and excessive internal mechanical friction, leading to an increased motor constant and

air leakage from the manifold. Consequently, the air compressor torque of the PEMFC supply system is adjusted by adding a linear term to the original torque. Based on these assumptions, the original tracking target is revised to reflect the constraints imposed by these fault conditions in the supply system [159].

Finally, to address these issues, a reconfigurable controller has been designed for the PEMFC system. This controller's fault tolerance and reconfiguration mechanisms (Figure 14a is based on fault factors, Figure 14b,c is based on observers) determine which backup controller is activated. The backup controller is then capable of regulating the cathode pressure and flow rate in response to faults.

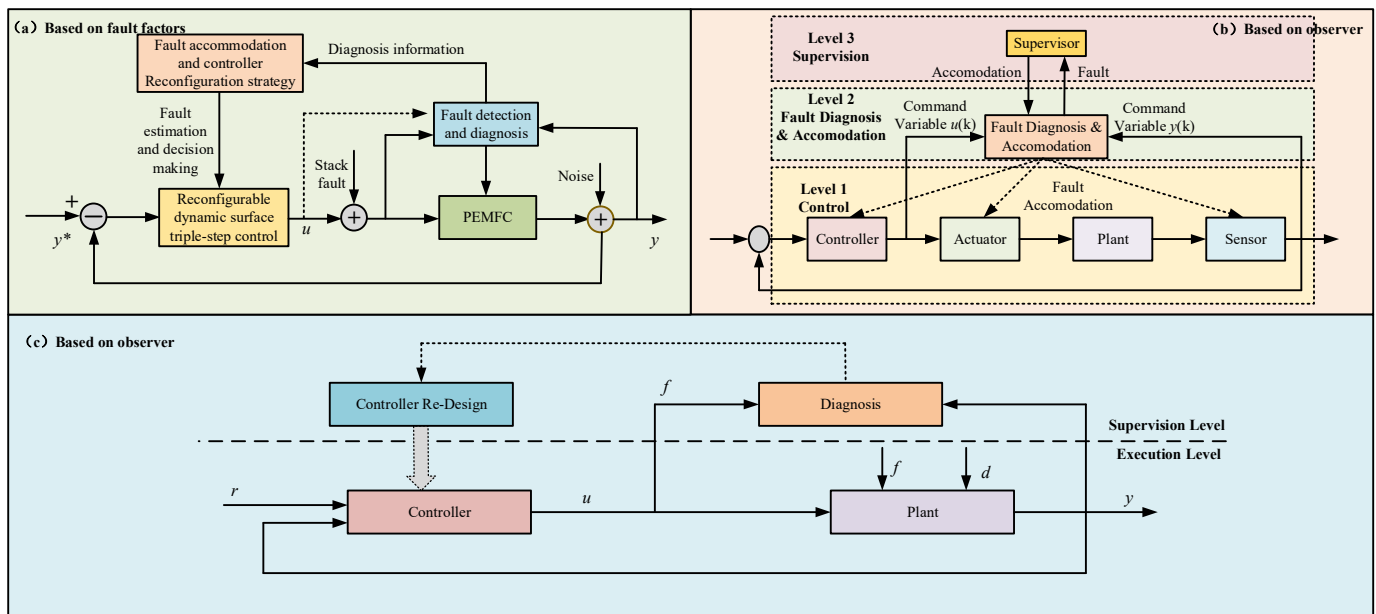


Figure 14. Selected Fault-tolerance mechanism.

7. Anode Control

There exist three distinct modes for anode supply systems: straight discharge, dead-end, and recirculation. The straight discharge mode has been disregarded due to its significant hydrogen wastage currently. In the dead-end mode, an exhaust valve is incorporated at the reactor's outlet, which is sealed post-reaction to harness the surplus hydrogen. However, this method has limitations as impurities and water cannot be effectively eliminated, leading to channel blockage and subsequent efficiency reduction. Consequently, researchers have increasingly concentrated their efforts on the recirculation mode of operation. This mode involves redirecting the surplus hydrogen back into the PEMFC stack via auxiliary components to facilitate hydrogen utilization, as shown in Figure 1c. Notably, the hydrogen circulation pump or elicitor stands out as the pivotal circulation apparatus in this hydrogen recirculation mode. It effectively circulates the unreacted hydrogen from the power reactor's anode outlet back to its anode inlet, ultimately boosting hydrogen utilization efficiency.

In the investigation of anode supply system control, researchers concentrate on the regulation of hydrogen flow and pressure. The management of hydrogen flow bears similarity to that of the cathode system, relying on a specific parameter correlation perturbation to optimize the power output of the PEMFC stack. However, the hydrogen recirculation mode introduces additional complexity, as it necessitates consideration of the hydrogen flow returning from the anode outlet. Consequently, the control system incorporates two actuators: the hydrogen recirculation pump and a solenoid valve. This ensures an adequate anode supply, maintains an optimal oxygen–hydrogen ratio, and maximizes the stack's output power. In response to load perturbations, these actuators are adjusted to regulate the recirculated hydrogen and the hydrogen supply from the storage device, respectively.

It is imperative to employ an appropriate multi-objective control algorithm for the effective regulation of the target actuator in the PEMFC anode supply system.

In recent years, there have been fewer publications on anode control compared to cathode control [162,163]. The primary reason is that anode control mainly focuses on the safety and economy of the PEMFC stack. Economic considerations are directed at the efficiency of hydrogen utilization.

Recent research has explored various control methods, including PID [164–166], PSO-PID control [167], fuzzy PID control [168], H-index control [169], SMC [170], MPC [171], reinforcement learning-based control [172], optimal control [173], fuzzy control [174], and neural network-based control [175]. The aforementioned control methods and their controller designs are described in the context of cathode supply control. Five distinct structures are presented in Figure 15, labeled as (a) PI controller, (b) ANN controller, (c) MPC, (d) DDPG controller, and (e) Hybrid controller. These controllers track the performance of the anode consistent with the cathode control.

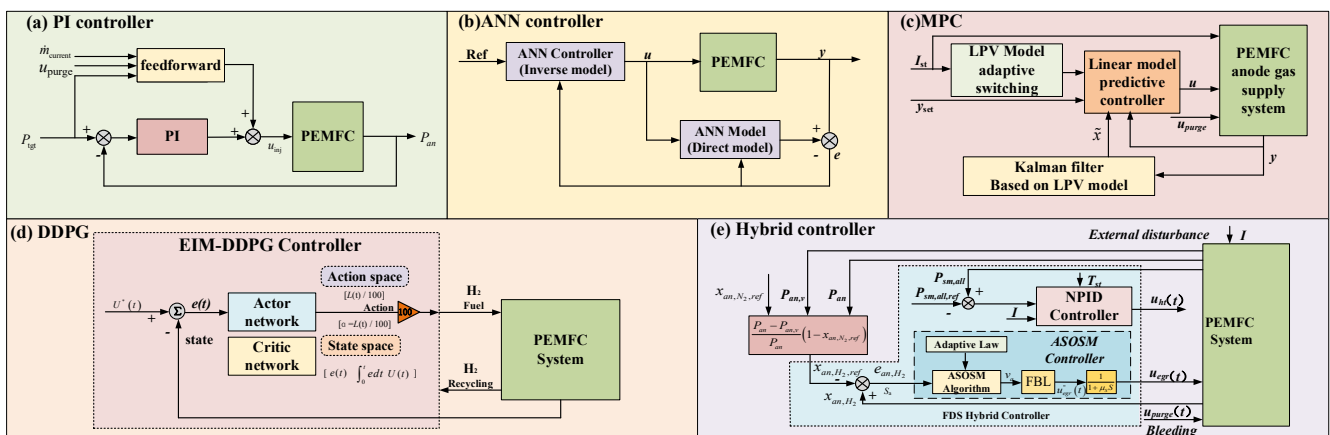


Figure 15. Structures for anode control method.

8. Coordinated Control of PEMFC

Coordinated PEMFC control is crucial for ensuring efficient and stable PEMFC operation under all load conditions by precisely regulating hydrogen and oxygen supplies, as well as temperature and moisture management.

As research has advanced, it has been discovered that pressure imbalances across the PEM can impact the fuel cell’s electrochemical reaction rate and potentially lead to irreversible damage. Consequently, based on studies of both the cathode and anode supply systems, a coordinated control strategy for managing cathode and anode pressures has been proposed to maintain dynamic equilibrium across the membrane. Meanwhile, the issue of pressure-induced two-phase flow can be optimized through this coordinated strategy.

What’s more, electrochemical reaction rates of PEMFC are primarily constrained by hydrogen transport through the PEM, influenced by stack temperature and membrane water content. Researchers are optimizing dynamic models by combining gas supply with hydrothermal management. Incorporating cathode and anode heat dissipation enhances thermal management accuracy and PEMFC efficiency. In PEMFC humidification, integrating humidification with the gas supply system allows for adjusting humidifier power based on humidity anomalies, maintaining optimal membrane water content for high system efficiency. Coordinated hydrothermal control is crucial for optimizing power stack dynamic performance.

The recently coordinated control includes a cathode and anode [176], oxygen and temperature [177], hydrogen and temperature [54], hydrogen and power [178], as well as cathode, temperature, and water [179]. Through the implementation of these coordinated control strategies, the operating efficiency of the fuel cell can be optimized and its service life can be extended, thereby enhancing both its economy and reliability.

Coordinated multi-objective control can further optimize operational performance and enhance system stability in PEMFCs compared to the separated anode or cathode control. The advantages of each coordinated combination are shown in Table 7. Although currently under-researched, coordinated multi-objective control is poised to become a focal point as the performance of PEMFC systems is further explored.

Table 7. Type of coordination.

Coordination Control Combination Type	Reasons and Benefits
Anode and Cathode Coordination Control, [176]	The primary goal is to balance the pressure difference between the two poles of the cell. Simultaneously, it optimizes gas utilization, reduces reaction losses, ensures stable battery output, and extends cell life.
Oxygen and Temperature Coordination Control, [177]	Temperature affects the diffusion speed of oxygen within the fuel cell and the kinetics of reactions. Proper temperature management can optimize oxygen utilization and reaction rates.
Hydrogen and Temperature Coordination Control, [54]	Temperature affects hydrogen's flow and reactivity. Maintaining an optimal temperature ensures efficient hydrogen utilization at the cathode, preventing accumulation or rapid consumption.
Hydrogen and Power Coordination Control, [178]	Power demand directly influences hydrogen consumption rates. Significant variations in battery load require adjustments in hydrogen supply to prevent shortages or excess.
Anode, Cathode, Temperature, and Water Coordination Control, [179]	Effective water production and removal are essential for maintaining ionic conductivity and temperature balance. Coordinated control prevents issues like cathode channel clogging and rapid water evaporation, ensuring optimal performance.

9. Conclusions and Discussion

This section presents a thorough overview, discussion, and assessment of the primary control strategies for PEMFC supply systems over the past decade. The analysis delves into various facets, including benefits, limitations, complexity, accuracy, robustness, and applicability. Key findings include the following:

- (i) **Controller Recommendations:** Given PEMFC system characteristics, modern controllers like SMC, NTSMC, and MPC, along with intelligent controllers such as DNC and SAC-based control, are recommended as shown in Figure 16, according to the evaluations in Figures 4, 6, 9 and 13 and Table 5. Their implementation should be customized for the application, incorporating observers and optimization algorithms.
- (ii) PEMFC is a complex, coupled nonlinear systems that require decoupling and linearization. This process results in higher computational complexity compared to a nonlinear controller. Meanwhile, due to the limited performance improvement of the H index control and optimal control, their application in the PEMFC supply system is not recommended. TSMC may encounter singularity issues; however, the use of NTSMC addresses these problems and further enhances performance.
- (iii) MPC relies on accurate model predictions to manage complex multivariable control tasks through solving online optimization problems, making it particularly suitable for a high-power PEMFC supply system. In contrast, SMC is valued for its simple structure and strong robustness to model uncertainties and external perturbations, making it appropriate for scenarios requiring maximum performance.
- (iv) DNC and SAC-based controls are recommended for intelligent controllers and these are usually model-free controls. The SAC algorithm exhibits the strongest performance among smart controllers. Additionally, composite algorithmic models demonstrate the best overall performance.
- (v) When using multiple optimization algorithms to refine controllers, improvements are often limited. Meanwhile, incorporating observers can further enhance performance, underscoring the importance of selecting the appropriate type of observer for each specific situation.

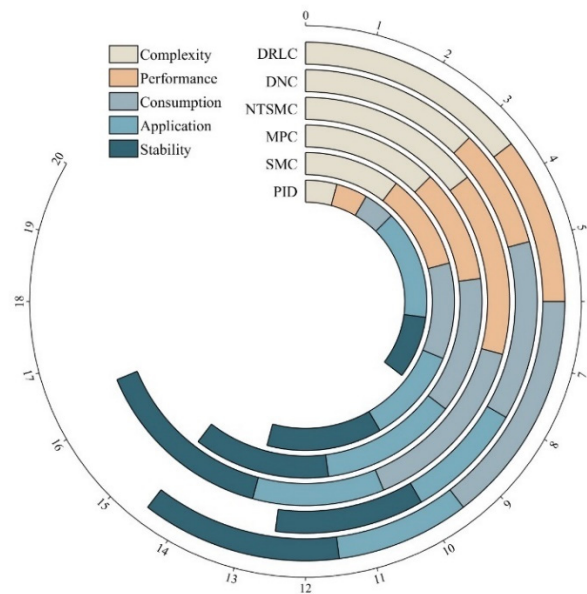


Figure 16. Recommended controllers' performance comparison.

10. Outlook

There are some promising prospects for future research in PEMFC supply systems, which are as follows:

- (i) Optimizing hydrogen supply under varying operating conditions and addressing delays and fluctuations in hydrogen supply are critical research issues. Currently, there is limited research focused on anode control. Investigating the use of suitable systems and control structures to optimize hydrogen supply and enhance fuel utilization remains a valuable area of study.
- (ii) Coordinated multi-objective control is poised to become a focal point as the performance of PEMFC systems is further explored. Therefore, Selecting the appropriate pairing of multiple controllers and co-optimizing between them presents a significant challenge.
- (iii) Model-free control based on intelligent controllers still has prospects with algorithm development. In particular, the development of new and improved deep reinforcement learning algorithms, as well as combinations of these algorithms, remains a focus of ongoing research.
- (iv) Fault-tolerant control is an underexplored area, including fault-tolerance considerations for air compressors, supply manifolds, and valves. Developing fault-tolerant mechanisms and strategies, along with designing actuating controllers, is of practical significance for PEMFC research.
- (v) Selecting appropriate algorithms and control strategies to optimize the PEMFC supply system, based on energy storage and load optimization, is also a significant area of interest.
- (vi) We recommend that, in addition to simulation and hardware-in-the-loop (HIL) testing, more experiments should be conducted under various conditions and environments to thoroughly assess the performance and stability of the controllers.

Funding: This research received no external funding. The APC was funded by [the National Natural Science Foundation of China] grant number [52205271].

Acknowledgments: We gratefully acknowledge the financial support from the National Natural Science Foundation of China (52205271).

Conflicts of Interest: The authors declare no conflict of interest.

Appendix A

Table A1. Cited controller performance indicators of cathode supply system.

Control Method	Tracking Performance			Output Voltage Index			Controller Structure and Complexity
	Rising Time (s)	Overshoot	Error (%)	Rising Time (s)	Overshoot (%)	Error (%)	
IAPPID, [84]	1.300	1.20	0.570	1.2	9.00	0.9000	Low
FuzzyPID, [80]	1.500	1.50	0.430	2.8	9.00	0.6870	Low
NNPID, [81]	1.480	1.30	0.520	/	/	/	Mid
Hybrid PID, [77]	1.480	1.60	0.480	/	/	/	Mid
Hybrid PID, [83]	1.840	1.30	0.420	2	0.00	0.6000	Mid
SMC, [90]	0.860	0.98	0.410	2.6	20.00	0.2800	Low
SMC with observer, [97]	0.380	0.89	0.063	1	9.00	0.3600	Mid
SMC with algorithm, [100]	0.330	0.63	0.060	0.6	0.00	0.3560	Mid
TSMC with observer, [180]	0.17	0.09	0.046	/	/	/	High
NTSMC with algorithm, [94]	0.09	0.06	0.008	0.452	2.30	0.0560	High
Optimal control with observer, [118]	1.200	1.03	0.530	5	8.60	0.8000	Mid
NN-MPC, [114]	0.134	0.11	0.016	/	/	/	High
MPC with observer, [116]	0.162	0.02	0.020	0.5	3.68	0.3800	Low
MPC, [181]	0.300	0.76	0.100	0.65	3.02	0.2600	Low
H index control, [119]	4.000	1.63	0.890	/	/	/	Low
FC with observer, [129]	0.720	0.30	0.612	/	/	/	Mid
FC, [130]	1.300	0.23	0.583	/	/	/	Low
DNC, [182]	0.800	0.75	0.080	4	4.60	0.3300	Low
DNC with observer, [140]	0.590	0.89	0.040	/	/	/	Mid
DDPG, [146]	0.150	0.40	0.070	/	/	/	High
FO-DDPG, [147]	0.015	0.01	0.602	/	/	/	High
SAC, [145]	0.070	0.51	0.067	0.9	2.60	0.2600	High
CIED-MD3, [143]	0.082	0.40	0.064	0.63	3.50	0.1680	High

Table A2. Cited controller performance indicators of anode supply system.

Control Method	Tracking Performance			Output Voltage Index			Controller Structure and Complexity
	Rising Time (s)	Overshoot (%)	Error (%)	Rising Time (s)	Overshoot (%)	Error (%)	
PI, [169]	0.90	0.67	0.78	/	/	/	Low
ANN, [175]	0.57	0.56	2.37	/	/	/	Low
MPC, [63]	0.40	0.18	0.03	/	/	/	Mid
DDPG, [172]	0.18	0.04	0.06	0.2	0.00	0.000068	Mid
SMC, [170]	10.60	0.05	0.60	12.6	0.02	0.110000	High

References

1. Omri, A.; Ben Jabeur, S. Climate Policies and Legislation for Renewable Energy Transition: The Roles of Financial Sector and Political Institutions. *Technol. Forecast. Soc. Chang.* **2024**, *203*, 123347. [[CrossRef](#)]

2. Ma, W.; Wang, W. Evolution of Renewable Energy Laws and Policies in China. *Heliyon* **2024**, *10*, e29712. [[CrossRef](#)] [[PubMed](#)]
3. Zha, D.; Jiang, P.; Zhang, C.; Xia, D.; Cao, Y. Positive Synergy or Negative Synergy: An Assessment of the Carbon Emission Reduction Effect of Renewable Energy Policy Mixes on China's Power Sector. *Energy Policy* **2023**, *183*, 113782. [[CrossRef](#)]
4. Hassan, M.; Kouzeze, M.; Lee, J.-Y.; Msolli, B.; Rjiba, H. Does Increasing Environmental Policy Stringency Enhance Renewable Energy Consumption in OECD Countries? *Energy Econ.* **2024**, *129*, 107198. [[CrossRef](#)]
5. Chen, L.; Ma, R. Clean Energy Synergy with Electric Vehicles: Insights into Carbon Footprint. *Energy Strategy Rev.* **2024**, *53*, 101394. [[CrossRef](#)]
6. Xu, C.; Zhuang, Y.; Qian, Y.; Cho, H. Effect on the Performance and Emissions of Methanol/Diesel Dual-Fuel Engine with Different Methanol Injection Positions. *Fuel* **2022**, *307*, 121868. [[CrossRef](#)]
7. Cao, J.; Wang, Y.; Dong, D.; Wei, F.; Zhang, H.; Jiang, L.; Dong, P.; Li, B.; Xiao, G.; Long, W. Over-Expansion Cycle as Clean Combustion Strategy Applied to a Marine Low-Speed Dual Fuel Engine. *J. Clean. Prod.* **2024**, *450*, 141958. [[CrossRef](#)]
8. Li, Y.; Ru, X.; Yang, M.; Zheng, Y.; Yin, S.; Hong, C.; Peng, F.; Qu, M.; Xue, C.; Lu, J.; et al. Flexible silicon solar cells with high power-to-weight ratios. *Nature* **2024**, *626*, 105–110. [[CrossRef](#)]
9. Calautit, K.; Johnstone, C. State-of-the-Art Review of Micro to Small-Scale Wind Energy Harvesting Technologies for Building Integration. *Energy Convers. Manag. X* **2023**, *20*, 100457. [[CrossRef](#)]
10. Kartal, M.T.; Kılıç Depren, S.; Ayhan, F.; Ulussever, T. Quantile-Based Heterogeneous Effects of Nuclear Energy and Political Stability on the Environment in Highly Nuclear Energy-Consuming and Politically Stable Countries. *Appl. Energy* **2024**, *365*, 123237. [[CrossRef](#)]
11. Wang, X.; Xia, H.; Guo, Y.; Duan, Y.; Wang, M.; Liu, Y.; Si, H. Research on Field Testing and Assessment Technology of Ocean Energy Converters. *Ocean Eng.* **2023**, *285*, 115539. [[CrossRef](#)]
12. Sadiq Okoh, A.; Chidi Onuoha, M. Immediate and Future Challenges of Using Electric Vehicles for Promoting Energy Efficiency in Africa's Clean Energy Transition. *Glob. Environ. Chang.* **2024**, *84*, 102789. [[CrossRef](#)]
13. Ağbulut, Ü.; Yıldız, G.; Bakır, H.; Polat, F.; Biçen, Y.; Ergün, A.; Gürel, A.E. Current Practices, Potentials, Challenges, Future Opportunities, Environmental and Economic Assumptions for Türkiye's Clean and Sustainable Energy Policy: A Comprehensive Assessment. *Sustain. Energy Technol. Assess.* **2023**, *56*, 103019. [[CrossRef](#)]
14. Islam, A.; Hossain, M.B.; Mondal, M.A.H.; Ahmed, M.T.; Hossain, M.A.; Monir, M.U.; Khan, M.F.H.; Islam, K.; Khandaker, S.; Choudhury, T.R.; et al. Energy Challenges for a Clean Environment: Bangladesh's Experience. *Energy Rep.* **2021**, *7*, 3373–3389. [[CrossRef](#)]
15. Guo, J.; Zhu, K.; Cheng, Y. Deployment of Clean Energy Technologies towards Carbon Neutrality under Resource Constraints. *Energy* **2024**, *295*, 131012. [[CrossRef](#)]
16. Shouwu, J.; Xu, T.; Shehzad, K.; Zaman, B.U.; Wuyue, L. The Role of Environmental Technologies and Clean Energy Transition in Shaping the N-Shaped Environmental Kuznets Curve: A North African Perspective. *Environ. Technol. Innov.* **2024**, *33*, 103463. [[CrossRef](#)]
17. Ling, W.; Liu, Y.; Young, R.; Cladouhos, T.T.; Jafarpour, B. Efficient Data-Driven Models for Prediction and Optimization of Geothermal Power Plant Operations. *Geothermics* **2024**, *119*, 102924. [[CrossRef](#)]
18. Ullah, A.; Altay Topcu, B.; Dogan, M.; Imran, M. Exploring the Nexus among Hydroelectric Power Generation, Financial Development, and Economic Growth: Evidence from the Largest 10 Hydroelectric Power-Generating Countries. *Energy Strategy Rev.* **2024**, *52*, 101339. [[CrossRef](#)]
19. Nchege, J.; Okpalaoka, C. Hydroelectric Production and Energy Consumption in Nigeria: Problems and Solutions. *Renew. Energy* **2023**, *219*, 119548. [[CrossRef](#)]
20. Irham, A.; Roslan, M.F.; Jern, K.P.; Hannan, M.A.; Mahlia, T.M.I. Hydrogen Energy Storage Integrated Grid: A Bibliometric Analysis for Sustainable Energy Production. *Int. J. Hydrogen Energy* **2024**, *63*, 1044–1087. [[CrossRef](#)]
21. Wang, L.L.; Xian, R.C.; Jiao, P.H.; Chen, J.J.; Chen, Y.; Liu, H.G. Multi-Timescale Optimization of Integrated Energy System with Diversified Utilization of Hydrogen Energy under the Coupling of Green Certificate and Carbon Trading. *Renew. Energy* **2024**, *228*, 120597. [[CrossRef](#)]
22. Xue, D.; Shao, Z. Patent Text Mining Based Hydrogen Energy Technology Evolution Path Identification. *Int. J. Hydrogen Energy* **2024**, *49*, 699–710. [[CrossRef](#)]
23. Guo, S.; Liu, J.; Zhao, C.; Wang, L.; Yang, Z. Research on Pre-Ignition in Hydrogen Internal Combustion Engines Based on Characteristic Parameters of Hot Spot. *Int. J. Hydrogen Energy* **2024**, *65*, 548–554. [[CrossRef](#)]
24. Dai, J.; Uwaneza, D.; Levstev, A.; Yu, Z.; Chen, D. Effect of the Geometric Parameters of the Rib-Channel and Porous Cathode on the Species Distribution in the Cathodes of Protonic Ceramic Fuel Cell Stack. *Int. J. Electrochem. Sci.* **2022**, *17*, 220116. [[CrossRef](#)]
25. Chen, D.; Zhu, Y.; Han, S.; Anatoly, L.; Andrey, M.; Lu, L. Investigate the Effect of a Parallel-Cylindrical Flow Field on the Solid Oxide Fuel Cell Stack Performance by 3D Multiphysics Simulating. *J. Energy Storage* **2023**, *60*, 106587. [[CrossRef](#)]
26. Wang, W.; Liu, J.; Serbin, S.; Chen, D.; Zhou, H. Thermal Stress Analysis for a Typical Planar Anode-Supported Fuel Cell Stack. *Sustain. Energy Technol. Assess.* **2022**, *54*, 102891. [[CrossRef](#)]
27. Zhang, G.; Yang, G.; Li, S.; Shen, Q.; Jiang, Z.; Li, Z.; Wang, H.; Liao, J.; Zhang, H. Molecular Dynamics Study on the Impacts of Cations in Sea Salt Aerosol on Transport Performance of Nafion Membranes for PEMFCs in Marine Application. *Int. J. Hydrogen Energy* **2022**, *47*, 27139–27149. [[CrossRef](#)]

28. Bagherabadi, K.M.; Skjong, S.; Bruinsma, J.; Pedersen, E. System-Level Modeling of Marine Power Plant with PEMFC System and Battery. *Int. J. Nav. Arch. Ocean Eng.* **2022**, *14*, 100487. [[CrossRef](#)]
29. Yang, J.; Wang, L.; Zhang, B.; Zhang, H.; Wu, X.; Xu, X.; Deng, P.; Peng, Y. Remaining Useful Life Prediction of Vehicle-Oriented PEMFC Systems Based on IGWO-BP Neural Network under Real-World Traffic Conditions. *Energy* **2024**, *291*, 130334. [[CrossRef](#)]
30. Xiao, C.; Wang, B.; Wang, C.; Yan, Y. Design of a Novel Fully-Active PEMFC-Lithium Battery Hybrid Power System Based on Two Automatic ON/OFF Switches for Unmanned Aerial Vehicle Applications. *Energy Convers. Manag.* **2023**, *292*, 117417. [[CrossRef](#)]
31. Li, Y.; Liu, Y.; Liang, Q.; Han, L.; Wan, N.; Guo, Z. Design and Performance Evaluation of an Air-Cooled PEMFC Stack with Metallic Bipolar Plates. *Int. J. Hydrogen Energy* **2024**, *60*, 324–332. [[CrossRef](#)]
32. Liu, J.; Chen, H.; Zhang, T. Analysis of Cold Start Characteristics in a PEMFC Stack with Different Current Loading Modes. *Int. J. Hydrogen Energy* **2024**, *51*, 1456–1476. [[CrossRef](#)]
33. Smith, G.; Sherin, B.; Goh, J.; Shinde, D.V. Fuel Cells—Proton-Exchange Membrane Fuel Cell | PEMFC: History, Introduction, Overview, Applications, Market. In *Reference Module in Chemistry, Molecular Sciences and Chemical Engineering*; Elsevier: Amsterdam, The Netherlands, 2023; ISBN 978-0-12-409547-2.
34. Cheng, M.; Liu, M.; Feng, Y.; Guo, Y.; Xu, H.; Luo, L.; Yin, J.; Yan, X.; Shen, S.; Zhang, J. Technical Challenges and Enhancement Strategies for Transitioning PEMFCs from H-Air to H-O₂. *Energy Convers. Manag.* **2024**, *311*, 118525. [[CrossRef](#)]
35. Pukrushpan, J.T. Modeling and Control of PEM Fuel Cell Systems and Fuel Processors. Ph.D. Dissertation, University of Michigan, Ann Arbor, MI, USA, 2003.
36. Yang, B.; Li, J.; Li, Y.; Guo, Z.; Zeng, K.; Shu, H.; Cao, P.; Ren, Y. A Critical Survey of Proton Exchange Membrane Fuel Cell System Control: Summaries, Advances, and Perspectives. *Int. J. Hydrogen Energy* **2022**, *47*, 9986–10020. [[CrossRef](#)]
37. Wu, D.; Peng, C.; Yin, C.; Tang, H. Review of System Integration and Control of Proton Exchange Membrane Fuel Cells. *Electrochem. Energ. Rev.* **2020**, *3*, 466–505. [[CrossRef](#)]
38. Daud, W.R.W.; Rosli, R.E.; Majlan, E.H.; Hamid, S.A.A.; Mohamed, R.; Husaini, T. PEM Fuel Cell System Control: A Review. *Renew. Energy* **2017**, *113*, 620–638. [[CrossRef](#)]
39. Lü, X.; Qu, Y.; Wang, Y.; Qin, C.; Liu, G. A Comprehensive Review on Hybrid Power System for PEMFC-HEV: Issues and Strategies. *Energy Convers. Manag.* **2018**, *171*, 1273–1291. [[CrossRef](#)]
40. George, S.; Sehgal, N.; Rana, K.P.S.; Kumar, V. A Comprehensive Review on Modelling and Maximum Power Point Tracking of PEMFC. *Clean. Energy Syst.* **2022**, *3*, 100031. [[CrossRef](#)]
41. Khan, M.J.; Iqbal, M.T. Modelling and Analysis of Electro-chemical, Thermal, and Reactant Flow Dynamics for a PEM Fuel Cell System. *Fuel Cells* **2005**, *5*, 463–475. [[CrossRef](#)]
42. Pan, M.; Li, C.; Liao, J.; Lei, H.; Pan, C.; Meng, X.; Huang, H. Design and Modeling of PEM Fuel Cell Based on Different Flow Fields. *Energy* **2020**, *207*, 118331. [[CrossRef](#)]
43. Mann, R.F.; Amphlett, J.C.; Hooper, M.A.; Jensen, H.M.; Peppley, B.A.; Roberge, P.R. Development and Application of a Generalised Steady-State Electrochemical Model for a PEM Fuel Cell. *J. Power Sources* **2000**, *86*, 173–180. [[CrossRef](#)]
44. Hu, D.; Wang, Y.; Li, J.; Yang, Q.; Wang, J. Investigation of Optimal Operating Temperature for the PEMFC and Its Tracking Control for Energy Saving in Vehicle Applications. *Energy Convers. Manag.* **2021**, *249*, 114842. [[CrossRef](#)]
45. H, S.K.; Abbas, Q.; Reichmann, K. Electrochemical Aspects of Interconnect Materials in PEMFCs. *Int. J. Hydrogen Energy* **2021**, *46*, 35420–35447. [[CrossRef](#)]
46. Zhou, H.; Wu, X.; Li, Y.; Fan, Z.; Chen, W.; Mao, J.; Deng, P.; Wik, T. Model Optimization of a High-Power Commercial PEMFC System via an Improved Grey Wolf Optimization Method. *Fuel* **2024**, *357*, 129589. [[CrossRef](#)]
47. Qiu, D.; Zhou, X.; Chen, M.; Xu, Z.; Peng, L. Optimization of Control Strategy for Air-Cooled PEMFC Based on in-Situ Observation of Internal Reaction State. *Appl. Energy* **2023**, *350*, 121752. [[CrossRef](#)]
48. Yang, Z.; Du, Q.; Jia, Z.; Yang, C.; Jiao, K. Effects of Operating Conditions on Water and Heat Management by a Transient Multi-Dimensional PEMFC System Model. *Energy* **2019**, *183*, 462–476. [[CrossRef](#)]
49. Lopes, D.G.; da Silva, E.P.; Pinto, C.S.; Neves, N.P.; Camargo, J.C.; Ferreira, P.F.P.; Furlan, A.L.; Lopes, D.G. Technical and Economic Analysis of a Power Supply System Based on Ethanol Reforming and PEMFC. *Renew. Energy* **2012**, *45*, 205–212. [[CrossRef](#)]
50. Zhang, X.; Xu, L.; Zou, L.; Jiang, Z.; Liao, J.; Gao, P.; Li, S.; Shen, Q. Modeling and Simulation of a Residential-Based PEMFC-CHP System. *Int. J. Electrochem. Sci.* **2024**, *19*, 100638. [[CrossRef](#)]
51. Silva, V.B.; Roubao, A. Hydrogen-Fed PEMFC: Overvoltage Analysis during an Activation Procedure. *J. Electroanal. Chem.* **2012**, *671*, 58–66. [[CrossRef](#)]
52. Zhu, H.; Wang, X.; Meng, W.; Ming, P.; Kong, F. Corrosion Behavior of Ti-Nb-Ni Foil as Bipolar Plates Substrate in Simulated PEMFC Solution: Effects of Fluoride Concentration and Temperature. *Fuel* **2024**, *362*, 130823. [[CrossRef](#)]
53. Yang, Y.; Bai, M.; Zhou, Z.; Wu, W.-T.; Hu, C.; Gao, L.; Li, Y.; Li, Y.; Song, Y. Numerical Simulation for Non-Uniform PtCo Catalyst Degradation under Constant Voltage Condition and Its Impact on PEMFC Performance. *Int. J. Heat Mass Transf.* **2024**, *218*, 124793. [[CrossRef](#)]
54. Chen, X.; Fang, Y.; Liu, Q.; He, L.; Zhao, Y.; Huang, T.; Wan, Z.; Wang, X. Temperature and Voltage Dynamic Control of PEMFC Stack Using MPC Method. *Energy Rep.* **2022**, *8*, 798–808. [[CrossRef](#)]
55. Wang, X.; Guo, Q.; Tu, C.; Che, L.; Hou, Y.; Xiao, F. A Two-Layer Control Strategy for Hydrogen-Battery Hybrid System Considering the Efficiency Characteristics of MS-PEMFC. *Electr. Power Syst. Res.* **2023**, *225*, 109818. [[CrossRef](#)]

56. Huang, W.; Jian, Q.; Feng, S.; Huang, Z. A Hybrid Optimization Strategy of Electrical Efficiency about Cooling PEMFC Combined with Ultra-Thin Vapor Chambers. *Energy Convers. Manag.* **2022**, *254*, 115301. [[CrossRef](#)]
57. Lu, Y.; Wang, X.; Yang, G.; Gong, D.; Xu, S. Experimental Study on the Influence of Operating Conditions on Performance Decline with Periodic Anode Purges in a Vehicular PEMFC Stack. *Int. J. Hydrogen Energy* **2024**, *69*, 1276–1286. [[CrossRef](#)]
58. Yang, G.; Meng, K.; Deng, Q.; Chen, W.; Chen, B. Numerical Investigation and Experimental Verification of Liquid Water Dynamic Transfer Characteristics in the Flow Field of PEMFC with Dead-Ended Anode during Gas Purging. *Chem. Eng. J.* **2024**, *491*, 152082. [[CrossRef](#)]
59. Zeng, L.; Li, Z. Fuel Cells—Proton-Exchange Membrane Fuel Cell | PEMFC: Anodes (Catalysts). In *Reference Module in Chemistry, Molecular Sciences and Chemical Engineering*; Elsevier: Amsterdam, The Netherlands, 2024; ISBN 978-0-12-409547-2.
60. Yin, R.-J.; Zeng, W.-C.; Bai, F.; Chen, L.; Tao, W.-Q. Study on the Effects of Manifold Structure on the Gas Flow Distribution Uniformity of Anode of PEMFC Stack with 140-Cell. *Renew. Energy* **2024**, *221*, 119693. [[CrossRef](#)]
61. Liu, S.; Chen, T.; Zhang, C.; Xie, Y. Study on the Performance of Proton Exchange Membrane Fuel Cell (PEMFC) with Dead-Ended Anode in Gravity Environment. *Appl. Energy* **2020**, *261*, 114454. [[CrossRef](#)]
62. Lin, H.; Jian, Q.; Bai, X.; Huang, W.; Feng, S. Mitigating Performance Deterioration Analysis of VC-PEMFC with Dead-Ended Anode by Pulsation Fuel Supplying Mode. *Int. J. Hydrogen Energy* **2023**, *48*, 10144–10159. [[CrossRef](#)]
63. Zhu, Y.; Zou, J.; Li, S.; Peng, C.; Xie, Y. Nonlinear Model Predictive Control of PEMFC Anode Hydrogen Circulation System Based on Dynamic Coupling Analysis. *Int. J. Hydrogen Energy* **2023**, *48*, 2385–2400. [[CrossRef](#)]
64. Abdollahzadeh, M.; Ribeirinha, P.; Boaventura, M.; Mendes, A. Three-Dimensional Modeling of PEMFC with Contaminated Anode Fuel. *Energy* **2018**, *152*, 939–959. [[CrossRef](#)]
65. Wang, F.-C.; Guo, Y.-F. Robustness Analyses of PEMFC Systems on the Production Line. *Int. J. Hydrogen Energy* **2015**, *40*, 1959–1966. [[CrossRef](#)]
66. Hong, L.; Chen, J.; Liu, Z.; Huang, L.; Wu, Z. A Nonlinear Control Strategy for Fuel Delivery in PEM Fuel Cells Considering Nitrogen Permeation. *Int. J. Hydrogen Energy* **2017**, *42*, 1565–1576. [[CrossRef](#)]
67. He, J.; Ahn, J.; Choe, S.-Y. Analysis and Control of a Fuel Delivery System Considering a Two-Phase Anode Model of the Polymer Electrolyte Membrane Fuel Cell Stack. *J. Power Sources* **2011**, *196*, 4655–4670. [[CrossRef](#)]
68. Wang, Y.; Wu, G.; Wang, Y. Modeling and Control for PEMFC Hydrogen Management Subsystem Based on Neural Network Compensation and Prescribed Tracking Accuracy. *Fuel* **2023**, *352*, 129019. [[CrossRef](#)]
69. Fan, L.; Liu, Y.; Luo, X.; Tu, Z.; Chan, S.H. A Novel Gas Supply Configuration for Hydrogen Utilization Improvement in a Multi-Stack Air-Cooling PEMFC System with Dead-Ended Anode. *Energy* **2023**, *282*, 129004. [[CrossRef](#)]
70. Gao, Y.; Lin, M. Research on the Performance Characteristics of Hydrogen Circulation Pumps for PEMFC Vehicles. *Int. J. Hydrogen Energy* **2024**, *50*, 1255–1272. [[CrossRef](#)]
71. Jin, J.; He, Z.; Zhao, X. Effect of Al Content on the Corrosion Resistance and Conductivity of Metal Nitride Coating in the Cathode Environment of PEMFCs. *Mater. Chem. Phys.* **2020**, *245*, 122739. [[CrossRef](#)]
72. Al-Dabbagh, A.W.; Lu, L.; Mazza, A. Modelling, Simulation and Control of a Proton Exchange Membrane Fuel Cell (PEMFC) Power System. *Int. J. Hydrogen Energy* **2010**, *35*, 5061–5069. [[CrossRef](#)]
73. Baroud, Z.; Benmiloud, M.; Benalia, A.; Ocampo-Martinez, C. Novel Hybrid Fuzzy-PID Control Scheme for Air Supply in PEM Fuel-Cell-Based Systems. *Int. J. Hydrogen Energy* **2017**, *42*, 10435–10447. [[CrossRef](#)]
74. Yu, J.; Yin, C.; Gong, X.; Yang, H.; Cao, J.; Tang, H. Research on Dynamic Internal Performance of PEMFC under Oxygen Starvation Using High-Resolution Segmented Cell Measurement. *Int. J. Hydrogen Energy* **2024**, *72*, 189–200. [[CrossRef](#)]
75. Borase, R.P.; Maghade, D.K.; Sondkar, S.Y.; Pawar, S.N. A review of PID control, tuning methods and applications. *Int. J. Dyn. Control* **2021**, *9*, 818–827. [[CrossRef](#)]
76. Swain, P.; Jena, D. PID Control Design for the Pressure Regulation of PEM Fuel Cell. In Proceedings of the 2015 International Conference on Recent Developments in Control, Automation and Power Engineering (RDCAPE), Noida, India, 12–13 March 2015; pp. 286–291.
77. Wei, L.; Zhu, X.; Wang, X.; Hu, Z.; Wang, M. Research on the Coordinated Control of Oxygen Excess Ratio and Air Pressure for PEMFC's Air Supply System. *Int. J. Hydrogen Energy* **2024**, *69*, 122–133. [[CrossRef](#)]
78. Divi, S.; Sonawane, S.H.; Das, S. Uncertainty analysis of transfer function of proton exchange membrane fuel cell and design of PI/PID controller for supply manifold pressure control. *Indian Chem. Eng.* **2018**, *61*, 138–152. [[CrossRef](#)]
79. Silaa, M.Y.; Barambones, O.; Bencherif, A. A Novel Adaptive PID Controller Design for a PEM Fuel Cell Using Stochastic Gradient Descent with Momentum Enhanced by Whale Optimizer. *Electronics* **2022**, *11*, 2610. [[CrossRef](#)]
80. Ou, K.; Wang, Y.-X.; Li, Z.-Z.; Shen, Y.-D.; Xuan, D.-J. Feedforward Fuzzy-PID Control for Air Flow Regulation of PEM Fuel Cell System. *Int. J. Hydrogen Energy* **2015**, *40*, 11686–11695. [[CrossRef](#)]
81. Damour, C.; Benne, M.; Lebreton, C.; Deseure, J.; Grondin-Perez, B. Real-Time Implementation of a Neural Model-Based Self-Tuning PID Strategy for Oxygen Stoichiometry Control in PEM Fuel Cell. *Int. J. Hydrogen Energy* **2014**, *39*, 12819–12825. [[CrossRef](#)]
82. AbouOmar, M.S.; Zhang, H.-J.; Su, Y.-X. Fractional Order Fuzzy PID Control of Automotive PEM Fuel Cell Air Feed System Using Neural Network Optimization Algorithm. *Energies* **2019**, *12*, 1435. [[CrossRef](#)]
83. Yue, H.; He, H.; Han, M.; Gong, S. An Unknown Input Nonlinear Observer Based Fractional Order PID Control of Fuel Cell Air Supply System. *Fuel* **2024**, *356*, 129619. [[CrossRef](#)]

84. Chen, Y.; Jiang, S.; Long, M.; Xu, J.; Liu, Y.; Kong, X.; Wan, Z. Optimization on the Peroxide Ratio Control Strategy of PEMFC System Based on Immune Algorithm. *Int. J. Hydrogen Energy* **2024**, *71*, 110–120. [[CrossRef](#)]
85. Jia, Y.; Zhang, R.; Zhang, T.; Fan, Z. Coordinated Control of the Fuel Cell Air Supply System Based on Fuzzy Neural Network Decoupling. *ACS Omega* **2021**, *6*, 34438–34446. [[CrossRef](#)] [[PubMed](#)]
86. Farhadi, P.; Sojoudi, T. PEMFC Voltage Control Using PSO-Tuned-PID Controller. In Proceedings of the 2014 IEEE NW Russia Young Researchers in Electrical and Electronic Engineering Conference, St. Petersburg, Russia, 3–5 February 2014; pp. 32–35.
87. Ahmadi, S.; Abdi, S.; Kakavand, M. Maximum Power Point Tracking of a Proton Exchange Membrane Fuel Cell System Using PSO-PID Controller. *Int. J. Hydrogen Energy* **2017**, *42*, 20430–20443. [[CrossRef](#)]
88. Wang, Y.; Li, H.; Feng, H.; Han, K.; He, S.; Gao, M. Simulation Study on the PEMFC Oxygen Starvation Based on the Coupling Algorithm of Model Predictive Control and PID. *Energy Convers. Manag.* **2021**, *249*, 114851. [[CrossRef](#)]
89. Baroud, Z.; Benmiloud, M.; Benalia, A. Sliding Mode Controller for Breathing Subsystem on a PEM Fuel Cell System. In Proceedings of the 2015 3rd International Conference on Control, Engineering & Information Technology (CEIT), Tlemcen, Algeria, 25–27 May 2015; pp. 1–6.
90. Ali, M.; Abudhahir, A.; ManivannaBoopathi, A. Sliding Mode Controller for Pressure Regulation in PEM Fuel Cell. *J. Commun. Technol. Electron. Comput. Sci.* **2017**, *15*, 5–15.
91. Li, C.; Jing, H.; Hu, J.; Hu, G.; Deng, Y. Sliding Mode Control for Power Tracking of Proton-Exchange Membrane Fuel-Cell System. *J. Energy Eng.* **2023**, *149*, 04023011. [[CrossRef](#)]
92. M., O.A.A.; Wang, H.; Tian, Y. Adaptive Integral Type-terminal Sliding Mode Control for PEMFC Air Supply System Using Time Delay Estimation Algorithm. *Asian J. Control* **2022**, *24*, 217–226. [[CrossRef](#)]
93. Napole, C.; Derbeli, M.; Barambones, O. A Global Integral Terminal Sliding Mode Control Based on a Novel Reaching Law for a Proton Exchange Membrane Fuel Cell System. *Appl. Energy* **2021**, *301*, 117473. [[CrossRef](#)]
94. Fang, S.; Zhang, R.; Maltsev, S.; Chen, D.; Fan, X.; Levstev, A. A Novel Adaptive Fast Sliding Mode Control Method Based on Fuzzy Algorithm for the Air Management System of Fuel Cell Stack. *Process Saf. Environ. Prot.* **2024**, *187*, 506–517. [[CrossRef](#)]
95. Feng, Y.; Yu, X.; Man, Z. Non-Singular Terminal Sliding Mode Control of Rigid Manipulators. *Automatica* **2002**, *38*, 2159–2167. [[CrossRef](#)]
96. Derbeli, M.; Barambones, O.; Farhat, M.; Ramos-Hernanz, J.A.; Sbita, L. Robust High Order Sliding Mode Control for Performance Improvement of PEM Fuel Cell Power Systems. *Int. J. Hydrogen Energy* **2020**, *45*, 29222–29234. [[CrossRef](#)]
97. Aykut Korkmaz, S.; Ayten Çetinkaya, S.; Yuksel, O.; Konur, O.; Emrah Erginer, K.; Ozgur Colpan, C. Fixed Time Adaptive Fault Tolerant Sliding Mode Control of PEMFC Air Supply System. *Int. J. Hydrogen Energy* **2024**, *51*, 1402–1420. [[CrossRef](#)]
98. Wang, Z.; Guo, X.; Dong, Z.; Cao, S. Finite-time Sliding Mode Fault-tolerant Control of PEM Fuel Cell Air Supply System. *Asian J. Control* **2024**, *26*, 3014–3026. [[CrossRef](#)]
99. Jiang, F.; Wei, Z.; Zhang, C.; He, H.; Song, R.; Gao, F. Cathodic Supply Optimization of PEMFC System Under Variable Altitude. *IEEE Trans. Ind. Electron.* **2024**, *71*, 14298–14307. [[CrossRef](#)]
100. Souissi, A. Adaptive sliding mode control of a PEM fuel cell system based on the super twisting algorithm. *Energy Rep.* **2021**, *7*, 3390–3399. [[CrossRef](#)]
101. Baroud, Z.; Benalia, A.; Ocampo-Martinez, C. Robust Fuzzy Sliding Mode Control for Air Supply on PEM Fuel Cell System. *Int. J. Model. Identif. Control* **2018**, *29*, 341–351. [[CrossRef](#)]
102. Wu, J.; Zhao, J.; Liu, Z.; Yang, H. Parameter estimation and control of a fuel cell air supply system based on an improved extended state observer. *Energy Sources Part A Recover. Util. Environ. Eff.* **2023**, *46*, 362–378. [[CrossRef](#)]
103. Yang, D.; Fu, H.; Li, J.; Wang, S. A Multivariable Sliding Mode Predictive Control Method for the Air Management System of Automotive Fuel Cells. *Meas. Control* **2024**, *57*, 139–151. [[CrossRef](#)]
104. Jing, H.; Huang, T.; Li, C.; Liu, X.; Hu, G.; Pang, C. Multi-Objective Sliding Mode Control of Proton Exchange Membrane Fuel Cell System Based on Adaptive Algebraic Observer. *Proc. Inst. Mech. Eng. Part A J. Power Energy* **2024**, *238*, 292–304. [[CrossRef](#)]
105. Liu, J.; Gao, Y.; Su, X.; Wack, M.; Wu, L. Disturbance-Observer-Based Control for Air Management of PEM Fuel Cell Systems via Sliding Mode Technique. *IEEE Trans. Control Syst. Technol.* **2019**, *27*, 1129–1138. [[CrossRef](#)]
106. Li, J.; Geng, J.; Yu, T. Multi-Objective Optimal Control for Proton Exchange Membrane Fuel Cell via Large-Scale Deep Reinforcement Learning. *Energy Rep.* **2021**, *7*, 6422–6437. [[CrossRef](#)]
107. Liu, Z.; Xu, S.; Shi, L. Research on PEMFC Cathode Circulation under Low-Load Conditions and Its Optimal Control in FCV Power System for Long-Term Durability. *Int. J. Hydrogen Energy* **2024**, *61*, 1015–1027. [[CrossRef](#)]
108. Barzegari, M.M.; Alizadeh, E.; Pahnabi, A.H. Grey-Box Modeling and Model Predictive Control for Cascade-Type PEMFC. *Energy* **2017**, *127*, 611–622. [[CrossRef](#)]
109. Afsharinejad, A.; Asemani, M.H.; Dehghani, M. Optimal Linear Parameter Varying Controller Design for Proton Exchange Membrane Fuel Cell Using LMI Techniques. In Proceedings of the 2020 28th Iranian Conference on Electrical Engineering (ICEE), Tabriz, Iran, 4–6 August 2020; IEEE: Piscataway, NJ, USA, 2020; pp. 1–5.
110. Fang, C.; Xu, L.; Li, J.; Ouyang, M. Feedback Linearization Based Air Pressure and Mass Flow Rate Regulation for PEMFCs. In Proceedings of the 2015 54th Annual Conference of the Society of Instrument and Control Engineers of Japan (SICE), Hangzhou, China, 28–30 July 2015; IEEE: Piscataway, NJ, USA, 2015; pp. 1321–1325.
111. Zhu, Y.; Xie, Y.; Zou, J.; Li, S. Near-Optimal Control of Net Output Power for PEMFC System. In Proceedings of the 2019 American Control Conference (ACC), Philadelphia, PA, USA, 10–12 July 2019; pp. 2801–2806.

112. Ziogou, C.; Voutetakis, S.; Georgiadis, M.C.; Papadopoulou, S. Model Predictive Control (MPC) Strategies for PEM Fuel Cell Systems—A Comparative Experimental Demonstration. *Chem. Eng. Res. Des.* **2018**, *131*, 656–670. [[CrossRef](#)]
113. Chatrattanawet, N.; Hakhen, T.; Kheawhom, S.; Arpornwichanop, A. Control Structure Design and Robust Model Predictive Control for Controlling a Proton Exchange Membrane Fuel Cell. *J. Clean. Prod.* **2017**, *148*, 934–947. [[CrossRef](#)]
114. Deng, Z.; Chen, M.; Wang, H.; Chen, Q. Performance-Oriented Model Learning and Model Predictive Control for PEMFC Air Supply System. *Int. J. Hydrogen Energy* **2024**, *64*, 339–348. [[CrossRef](#)]
115. Yang, D.; Pan, R.; Wang, Y.; Chen, Z. Modeling and Control of PEMFC Air Supply System Based on TS Fuzzy Theory and Predictive Control. *Energy* **2019**, *188*, 116078. [[CrossRef](#)]
116. Jiang, W.; Zhu, Z.; Li, C.; Cheng, Z.; Zheng, Z. Observer-Based Model Predictive Control Design for Air Supply System of Automotive PEM Fuel Cells. In Proceedings of the 2020 39th Chinese Control Conference (CCC), Shenyang, China, 27–29 July 2020; IEEE: Piscataway, NJ, USA, 2020; pp. 5413–5418.
117. Ouyang, Q.; Chen, J.; Wang, F.; Su, H. Nonlinear MPC Controller Design for AIR Supply of PEM Fuel Cell Based Power Systems. *Asian J. Control* **2017**, *19*, 929–940. [[CrossRef](#)]
118. Zhu, Y.; Zou, J.; Li, S.; Peng, C. An Adaptive Sliding Mode Observer Based Near-Optimal OER Tracking Control Approach for PEMFC under Dynamic Operation Condition. *Int. J. Hydrogen Energy* **2022**, *47*, 1157–1171. [[CrossRef](#)]
119. Wang, F.-C.; Lin, L.-H.; Chou, M.-C. Multivariable Robust Control for a 500W Self-Humidified PEMFC System. *Eur. J. Control* **2011**, *17*, 429–441. [[CrossRef](#)]
120. Wang, F.-C.; Chen, H.-T. Design and Implementation of Fixed-Order Robust Controllers for a Proton Exchange Membrane Fuel Cell System. *Int. J. Hydrogen Energy* **2009**, *34*, 2705–2717. [[CrossRef](#)]
121. Wang, F.-C.; Chen, H.-T.; Yang, Y.-P.; Yen, J.-Y. Multivariable Robust Control of a Proton Exchange Membrane Fuel Cell System. *J. Power Sources* **2008**, *177*, 393–403. [[CrossRef](#)]
122. Wang, F.-C.; Yang, Y.-P.; Chang, H.-P.; Ma, Y.-W.; Huang, C.-W.; Weng, B.-J. Proton Exchange Membrane Fuel Cell System Identification and Control: Part II—H-Infinity Based Robust Control. In Proceedings of the International Conference on Fuel Cell Science, Engineering and Technology, Irvine, CA, USA, 19–21 June 2006; Volume 42479, pp. 1105–1110.
123. Liu, Y.; Qie, T.; Yu, Y.; Wang, Y.; Chau, T.K.; Zhang, X.; Manandhar, U.; Iu, H.H.; Fernando, T. A Novel Integral Reinforcement Learning-Based H_∞ Control Strategy for Proton Exchange Membrane Fuel Cell in DC Microgrids. *IEEE Trans. Smart Grid* **2022**, *14*, 1668–1681. [[CrossRef](#)]
124. Gheisarnejad, M.; Boudjadar, J.; Khooban, M.H. A new adaptive type-II fuzzy-based deep reinforcement learning control: Fuel cell air-feed sensors control. *IEEE Sens. J.* **2019**, *19*, 9081–9089. [[CrossRef](#)]
125. Zhou, J.; Liao, Y.; Liu, J.; Xue, Y.; Xue, S. Deep Reinforcement Learning Guided Cascade Control for Air Supply of Polymer Exchange Membrane Fuel Cell. *Energy Technol.* **2021**, *9*, 2100149. [[CrossRef](#)]
126. Li, J.; Yu, T.; Yang, B. Adaptive Controller of PEMFC Output Voltage Based on Ambient Intelligence Large-Scale Deep Reinforcement Learning. *IEEE Access* **2021**, *9*, 6063–6075. [[CrossRef](#)]
127. Li, J.; Yu, T. A New Adaptive Controller Based on Distributed Deep Reinforcement Learning for PEMFC Air Supply System. *Energy Rep.* **2021**, *7*, 1267–1279. [[CrossRef](#)]
128. Zhang, H.K.; Wang, Y.F.; Wang, D.H.; Wang, Y.L. Adaptive Robust Control of Oxygen Excess Ratio for PEMFC System Based on Type-2 Fuzzy Logic System. *Inf. Sci.* **2020**, *511*, 1–17. [[CrossRef](#)]
129. Wang, Y.; Wang, Y.; Wang, D.; Chai, T. Observer-based composite adaptive type-2 fuzzy control for PEMFC air supply systems. *IEEE Trans. Fuzzy Syst.* **2020**, *30*, 515–529. [[CrossRef](#)]
130. Luo, G.; Ma, B.; Wang, Z.; Yin, L.; Wang, Y. Model-free adaptive control for the PEMFC air supply system based on interval type-2 fuzzy logic systems. *J. Renew. Sustain. Energy* **2020**, *12*, 064301. [[CrossRef](#)]
131. Derbeli, M.; Napole, C.; Barambones, O. Machine Learning Approach for Modeling and Control of a Commercial Heliocentris FC50 PEM Fuel Cell System. *Mathematics* **2021**, *9*, 2068. [[CrossRef](#)]
132. Liu, Y.; Xiao, C.; Wu, W.; Wan, Y.; Chen, J. PEMFC System Modeling and Control of Oxygen Excess Ratio in Air Supply Systems. In Proceedings of the 2023 China Automation Congress (CAC), Chongqing, China, 17–19 November 2023; IEEE: Piscataway, NJ, USA, 2023; pp. 2762–2767.
133. Sanchez, V.M.; Barbosa, R.; Arriaga, L.G.; Ramirez, J.M. Real Time Control of Air Feed System in a PEM Fuel Cell by Means of an Adaptive Neural-Network. *Int. J. Hydrogen Energy* **2014**, *39*, 16750–16762. [[CrossRef](#)]
134. Wang, Y.; Wang, Y. Pressure and Oxygen Excess Ratio Control of PEMFC Air Management System Based on Neural Network and Prescribed Performance. *Eng. Appl. Artif. Intell.* **2023**, *121*, 105850. [[CrossRef](#)]
135. Rezazadeh, A.; Askarzadeh, A.; Sedighizadeh, M. Adaptive Inverse Control of Proton Exchange Membrane Fuel Cell Using RBF Neural Network. *Int. J. Electrochem. Sci.* **2011**, *6*, 3105–3117. [[CrossRef](#)]
136. da Costa Lopes, F.; Watanabe, E.H.; Rolim, L.G.B. A Control-Oriented Model of a PEM Fuel Cell Stack Based on NARX and NOE Neural Networks. *IEEE Trans. Ind. Electron.* **2015**, *62*, 5155–5163. [[CrossRef](#)]
137. Wang, Y.-L.; Wang, Y.-F.; Zhang, H.-K. Robust Adaptive Control of PEMFC Air Supply System Based on Radical Basis Function Neural Network. *J. Dyn. Syst. Meas. Control* **2019**, *141*, 064503. [[CrossRef](#)]
138. Abbaspour, A.; Khalilnejad, A.; Chen, Z. Robust Adaptive Neural Network Control for PEM Fuel Cell. *Int. J. Hydrogen Energy* **2016**, *41*, 20385–20395. [[CrossRef](#)]

139. Li, P.; Chen, J.; Cai, T.; Zhang, B. Adaptive Control of Air Delivery System for PEM Fuel Cell Using Backstepping. In Proceedings of the 2011 8th Asian Control Conference (ASCC), Kaohsiung, Taiwan, 15–18 May 2011; IEEE: Piscataway, NJ, USA, 2011; pp. 1282–1287.
140. Wang, Y.; Wang, Y.; Xu, J.; Chai, T. Observer-Based Discrete Adaptive Neural Network Control for Automotive PEMFC Air-Feed Subsystem. *IEEE Trans. Veh. Technol.* **2021**, *70*, 3149–3163. [[CrossRef](#)]
141. Wang, Y.; Wang, Y.; Chen, G. Robust Composite Adaptive Neural Network Control for Air Management System of PEM Fuel Cell Based on High-Gain Observer. *Neural Comput. Appl.* **2020**, *32*, 10229–10243. [[CrossRef](#)]
142. Li, J.; Yu, T.; Yang, B. Coordinated Control of Gas Supply System in PEMFC Based on Multi-Agent Deep Reinforcement Learning. *Int. J. Hydrogen Energy* **2021**, *46*, 33899–33914. [[CrossRef](#)]
143. Li, J.; Yu, T. Intelligent Controller Based on Distributed Deep Reinforcement Learning for PEMFC Air Supply System. *IEEE Access* **2021**, *9*, 7496–7507. [[CrossRef](#)]
144. Li, J.; Yu, T. Sensors Integrated Control of PEMFC Gas Supply System Based on Large-Scale Deep Reinforcement Learning. *Sensors* **2021**, *21*, 349. [[CrossRef](#)] [[PubMed](#)]
145. Su, Q.; Zhou, J.; Yi, F.; Hu, D.; Lu, D.; Wu, G.; Zhang, C.; Deng, B.; Cao, D. An Intelligent Control Method for PEMFC Air Supply Subsystem to Optimize Dynamic Response Performance. *Fuel* **2024**, *361*, 130697. [[CrossRef](#)]
146. Pan, L.; Zhang, T.; Gao, Y. Real-Time Control of Gas Supply System for a PEMFC Cold-Start Based on the MADDPG Algorithm. *Energies* **2023**, *16*, 4655. [[CrossRef](#)]
147. Yuan, H.; Sun, Z.; Wang, Y.; Chen, Z. Deep Reinforcement Learning Algorithm Based on Fusion Optimization for Fuel Cell Gas Supply System Control. *World Electr. Veh. J.* **2023**, *14*, 50. [[CrossRef](#)]
148. Wang, G.; Wang, X.; Wang, L.; Jia, L.; Shao, M.; Yu, Y. Multi-Agent Reinforcement Learning Based Coordinated Control of PEMFC Gas Supply System. In Proceedings of the 2022 IEEE 17th Conference on Industrial Electronics and Applications (ICIEA), Chengdu, China, 16–19 December 2022; pp. 132–137.
149. Li, J.; Yu, T. Large-Scale Multi-Agent Deep Reinforcement Learning-Based Coordination Strategy for Energy Optimization and Control of Proton Exchange Membrane Fuel Cell. *Sustain. Energy Technol. Assess.* **2021**, *48*, 101568. [[CrossRef](#)]
150. Yildirim, B.; Gheisarnejad, M.; Özdemir, M.T.; Khooban, M.H. Multi-Agent Fuzzy Q-Learning-Based PEM Fuel Cell Air-Feed System Control. *Int. J. Hydrogen Energy* **2024**, *75*, 354–362. [[CrossRef](#)]
151. Cecilia, A.; Serra, M.; Costa-Castelló, R. PEMFC State and Parameter Estimation through a High-Gain Based Adaptive Observer. *IFAC-Pap.* **2020**, *53*, 5895–5900. [[CrossRef](#)]
152. Yuan, H.; Dai, H.; Wei, X.; Ming, P. A Novel Model-Based Internal State Observer of a Fuel Cell System for Electric Vehicles Using Improved Kalman Filter Approach. *Appl. Energy* **2020**, *268*, 115009. [[CrossRef](#)]
153. Hernández-gómez, Á.; Langarica-Cordoba, D.; Martínez-Rodríguez, P.R.; González-Aguilar, H.; Guilbert, D.; Saldivar, B. Design and Implementation of the Luenberger Observer for Estimating the Voltage Response of a PEM Electrolyzer During Supply Current Variations. *IEEE Access* **2024**, *12*, 68266–68277. [[CrossRef](#)]
154. Zakaria, B.; Noureddine, G.; Atallah, B.; Carlos, O. Algebraic Observer-based Output-feedback Controller Design for a PEM Fuel Cell Air-supply Subsystem. *IET Renew. Power Gener.* **2018**, *12*, 1714–1721. [[CrossRef](#)]
155. Puig, V.; Feroldi, D.; Serra, M.; Quevedo, J.; Riera, J. Fault-Tolerant MPC Control of PEM Fuel Cells. *IFAC Proc. Vol.* **2008**, *41*, 11112–11117. [[CrossRef](#)]
156. Ingimundarson, A.; Peña, R.S.S. Using the Unfalsified Control Concept to Achieve Fault Tolerance. *IFAC Proc. Vol.* **2008**, *41*, 1236–1242. [[CrossRef](#)]
157. Liu, J.; Luo, W.; Yang, X.; Wu, L. Robust model-based fault diagnosis for PEM fuel cell air-feed system. *IEEE Trans. Ind. Electron.* **2016**, *63*, 3261–3270. [[CrossRef](#)]
158. Wang, Y.; Li, M.; Gao, J.; Chu, H.; Chen, H. Fault-Tolerant Control through Dynamic Surface Triple-Step Approach for Proton Exchange Membrane Fuel Cell Air Supply Systems. *Int. J. Hydrogen Energy* **2022**, *47*, 1804–1819. [[CrossRef](#)]
159. Guo, X.; Fan, N.; Dong, Z.; Wang, C. Adaptive prescribed performance control for PEM fuel cell air supply systems with unknown air compressor faults. *IEEE Trans. Ind. Electron.* **2023**, *71*, 7664–7672. [[CrossRef](#)]
160. Bianchi, F.D.; Ocampo-Martinez, C.; Kunusch, C.; Sánchez-Peña, R.S. Fault-Tolerant Unfalsified Control for PEM Fuel Cell Systems. *IEEE Trans. Energy Convers.* **2015**, *30*, 307–315. [[CrossRef](#)]
161. Yang, D.; Wang, Y.; Chen, Z. Robust Fault Diagnosis and Fault Tolerant Control for PEMFC System Based on an Augmented LPV Observer. *Int. J. Hydrogen Energy* **2020**, *45*, 13508–13522. [[CrossRef](#)]
162. Bao, C.; Ouyang, M.; Yi, B. Modeling and Control of Air Stream and Hydrogen Flow with Recirculation in a PEM Fuel Cell System—II. Linear and Adaptive Nonlinear Control. *Int. J. Hydrogen Energy* **2006**, *31*, 1897–1913. [[CrossRef](#)]
163. Wu, B.; Matian, M.; Offer, G.J. Hydrogen PEMFC System for Automotive Applications. *Int. J. Low-Carbon Technol.* **2012**, *7*, 28–37. [[CrossRef](#)]
164. Zambri, N.A.; Salim, N.B.; Noh, F.H.M.; Yi, S.S. Performance Comparison of PEMFC Hydrogen Reformer with Different Controllers. *TELKOMNIKA (Telecommun. Comput. Electron. Control.)* **2019**, *17*, 2617–2624. [[CrossRef](#)]
165. Rosli, R.E.; Majlan, E.H.; Wan Daud, W.R.; Hamid, S.A.A. Hydrogen Rate Manipulation of Proton Exchange Membrane Fuel Cell (PEMFC) Stack Using Feedback Control System. In Proceedings of the 2012 IEEE International Conference on Power and Energy (PECon), Kota Kinabalu, Malaysia, 2–5 December 2012; pp. 553–557.

166. Qin, B.; Wang, X.; Wang, L.; Zhao, H.; Yin, X.; Jia, L. Hydrogen Excess Ratio Control of Ejector-Based Hydrogen Recirculation PEM Fuel Cell System. In Proceedings of the 2019 34rd Youth Academic Annual Conference of Chinese Association of Automation (YAC), Jinzhou, China, 6–8 June 2019; pp. 648–653.
167. Xue, H.; Zhang, H.; Sun, W.; Yao, A.; Jia, L. An Optimized Fuzzy PI Control Method Utilizing an Improved QPSO for the Hydrogen Supply of PEMFC. In Proceedings of the 2023 IEEE 18th Conference on Industrial Electronics and Applications (ICIEA), Ningbo, China, 18–22 August 2023; pp. 603–608.
168. Yuan, H.; Dai, H.; Wu, W.; Xie, J.; Shen, J.; Wei, X. A Fuzzy Logic PI Control with Feedforward Compensation for Hydrogen Pressure in Vehicular Fuel Cell System. *Int. J. Hydrogen Energy* **2021**, *46*, 5714–5728. [[CrossRef](#)]
169. Fang, C.; Li, J.; Xu, L.; Ouyang, M.; Hu, J.; Cheng, S. Model-Based Fuel Pressure Regulation Algorithm for a Hydrogen-Injected PEM Fuel Cell Engine. *Int. J. Hydrogen Energy* **2015**, *40*, 14942–14951. [[CrossRef](#)]
170. Deng, H.; Chen, W.; Cao, D.; Chen, J.; Hu, W. Uncertainty Analysis and Robust Control of Fuel Delivery Systems Considering Nitrogen Crossover Phenomenon. *Int. J. Hydrogen Energy* **2020**, *45*, 32367–32387. [[CrossRef](#)]
171. Quan, S.; Wang, Y.-X.; Xiao, X.; He, H.; Sun, F. Feedback Linearization-Based MIMO Model Predictive Control with Defined Pseudo-Reference for Hydrogen Regulation of Automotive Fuel Cells. *Appl. Energy* **2021**, *293*, 116919. [[CrossRef](#)]
172. Li, J.; Yu, T. Distributed Deep Reinforcement Learning for Optimal Voltage Control of PEMFC. *IET Renew. Power Gener.* **2021**, *15*, 2778–2798. [[CrossRef](#)]
173. Chen, L.; Xu, K.; Yang, Z.; Yan, Z.; Dong, Z. Optimal Design and Operation of Dual-Ejector PEMFC Hydrogen Supply and Circulation System. *Energies* **2022**, *15*, 5427. [[CrossRef](#)]
174. Bouchouia, N.E.; Derghal, A.; Mahmah, B.; Madi, B.; Khochemane, L.; Hadjadj Aoul, E. An Adaptive Fuzzy Logic Controller (AFLC) for PEMFC Fuel Cell. *Int. J. Hydrogen Energy* **2015**, *40*, 13806–13819. [[CrossRef](#)]
175. Morán-Durán, A.; Martínez-Sibaja, A.; Rodríguez-Jarquín, J.P.; Posada-Gómez, R.; González, O.S. PEM Fuel Cell Voltage Neural Control Based on Hydrogen Pressure Regulation. *Processes* **2019**, *7*, 434. [[CrossRef](#)]
176. Zhang, X.; Zhang, C.; Zhang, Z.; Gao, S.; Li, H. Coordinated Management of Oxygen Excess Ratio and Cathode Pressure for PEMFC Based on Synthesis Variable-Gain Robust Predictive Control. *Appl. Energy* **2024**, *367*, 123415. [[CrossRef](#)]
177. Song, D.; Wu, Q.; Zeng, X.; Zhang, X.; Qian, Q.; Yang, D. Feedback-Linearization Decoupling Based Coordinated Control of Air Supply and Thermal Management for Vehicular Fuel Cell System. *Energy* **2024**, *305*, 132347. [[CrossRef](#)]
178. Li, J.; Cui, H.; Jiang, W.; Yu, H. A Large-Scale Multi-Agent Deep Reinforcement Learning Method for Cooperative Output Voltage Control of PEMFCs. *IEEE Trans. Transp. Electrif.* **2024**, *10*, 78–94. [[CrossRef](#)]
179. Ahn, J.-W.; He, J.; Choe, S.-Y. Design of Air, Water, Temperature and Hydrogen Controls for a PEM Fuel Cell System. In Proceedings of the ASME 2011 9th International Conference on Fuel Cell Science, Engineering and Technology collocated with ASME 2011 5th International Conference on Energy Sustainability, Washington, DC, USA, 7–10 August 2011.
180. Duan, F.; Kang, Z. Oxygen Excess Ratio Feedforward Control Based on ESO for PEMFC in DC Off-Grid Hydrogen Production Systems. *Int. J. Hydrogen Energy* **2024**, *77*, 347–358. [[CrossRef](#)]
181. Gruber, J.K.; Doll, M.; Bordons, C. Design and Experimental Validation of a Constrained MPC for the Air Feed of a Fuel Cell. *Control Eng. Pract.* **2009**, *17*, 874–885. [[CrossRef](#)]
182. Sánchez, V.; Ramírez, J.M.; Arriaga, G. On-Line Air Supply Control of PEM Fuel Cell by an Adaptive Neural Network. In Proceedings of the North American Power Symposium, Arlington, TX, USA, 26–28 September 2010; IEEE: Piscataway, NJ, USA, 2010; pp. 1–6.

Disclaimer/Publisher's Note: The statements, opinions and data contained in all publications are solely those of the individual author(s) and contributor(s) and not of MDPI and/or the editor(s). MDPI and/or the editor(s) disclaim responsibility for any injury to people or property resulting from any ideas, methods, instructions or products referred to in the content.